



TRANSPARENT TESTA GLABRA2 defines trichome cell shape by modulating actin cytoskeleton in *Arabidopsis thaliana*

Lu Liu ^{1,†} Yali Wang ^{1,†} Weihua Cao ¹ Lan Yang ¹ Chi Zhang ¹ Lanxin Yuan ¹ Dan Wang ¹
Wenja Wang ² Hongchang Zhang ¹ John Schiefelbein ³ Fei Yu ¹ Lijun An ^{1,*}

- 1 State Key Laboratory of Crop Stress Biology for Arid Areas and College of Life Sciences, Northwest A&F University, Yangling, Shaanxi 712100, China
- 2 CAS Center for Excellence in Molecular Plant Sciences, Chinese Academy of Sciences, Shanghai 200032, China
- 3 Department of Molecular, Cellular, and Developmental Biology, University of Michigan, Ann Arbor, MI 48109, USA

*Author for correspondence: lijunan@nwsuaf.edu.cn

[†]These authors are co-first author and contributed equally (L.L., Y.W.).

The author responsible for distribution of materials integral to the findings presented in this article in accordance with the policy described in the Instructions for Authors (<https://academic.oup.com/plphys/pages/General-Instructions>) is: Lijun An.

Abstract

The *Arabidopsis thaliana* *TRANSPARENT TESTA GLABRA2* (*TTG2*) gene encodes a WRKY transcription factor that regulates a range of development events like trichome, seed coat, and atrichoblast formation. Loss-of-function of *TTG2* was previously shown to reduce or eliminate trichome specification and branching. Here, we report the identification of an allele of *TTG2*, *ttg2-6*. In contrast to the *ttg2* mutants described before, *ttg2-6* displayed unique trichome phenotypes. Some *ttg2-6* mutant trichomes were hyper-branched, whereas others were hypo-branched, distorted, or clustered. Further, we found that in addition to specifically activating R3 MYB transcription factor TRIPTYCHON (TRY) to modulate trichome specification, *TTG2* also integrated cytoskeletal signaling to regulate trichome morphogenesis. The *ttg2-6* trichomes displayed aberrant cortical microtubules (cMTs) and actin filaments (F-actin) configurations. Moreover, genetic and biochemical analyses showed that *TTG2* could directly bind to the promoter and regulate the expression of *BRICK1* (*BRK1*), which encodes a subunit of the actin nucleation promoting complex suppressor of cyclic AMP repressor (SCAR)/Wiskott–Aldrich syndrome protein family verprolin homologous protein (WAVE). Collectively, taking advantage of *ttg2-6*, we uncovered a function for *TTG2* in facilitating cMTs and F-actin cytoskeleton-dependent trichome development, providing insight into cellular signaling events downstream of the core transcriptional regulation during trichome development in *Arabidopsis*.

Introduction

Trichomes are specialized epidermal structures in plants and have long been favored as a model system to elaborate cell differentiation and morphogenesis in plants due to their unique developmental patterns (Hülkamp 2004; Li et al. 2019; Arteaga et al. 2022; Li et al. 2023). In *Arabidopsis thaliana*, the leaf trichomes are single-celled structures, and usually exhibit as a well-extended stalk crowned with 3 or 4

straight branches (Hülkamp et al. 1994; Folkers et al. 1997). They are also well arranged in spatial distributions, and clustered trichomes are rare (Hülkamp et al. 1994). The formation of such unique patterning forms and architecture depend on a group of key genetic factors.

TRANSPARENT TESTA GLABRA2 (*TTG2*) encodes a WRKY transcription factor that plays important roles during trichome development (Johnson et al. 2002). Inactivation of *TTG2* leads to pleiotropic trichome developmental defects

Received November 30, 2023. Accepted January 17, 2024. Advance access publication February 23, 2024.

© The Author(s) 2024. Published by Oxford University Press on behalf of American Society of Plant Biologists. All rights reserved. For commercial re-use, please contact reprints@oup.com for reprints and translation rights for reprints. All other permissions can be obtained through our RightsLink service via the Permissions link on the article page on our site—for further information please contact journals.permissions@oup.com.

including clustered trichomes, reduced trichome density, and abnormal trichome branches (Johnson et al. 2002), implying *TTG2* may participate in multiple regulatory pathways to control trichome development. Current information indicate that the temporal and spatial expression of *TTG2* is directly regulated by the transcriptional activation complex comprised of the R2R3 MYB protein *GLABRA 1* (*GL1*), the basic helix-loop-helix (bHLH) proteins *GLABRA 3* (*GL3*) and *ENHANCER OF GL3* (*EGL3*), and the WD repeat protein *TTG1* (Johnson et al. 2002; Ishida et al. 2007; Zhao et al. 2008). They are considered to be the first tier positive regulators for trichome initiation (Morohashi and Grotewold 2009), and mutation of each of them results in glabrous or decreased trichome numbers (Tominaga-Wada et al. 2011; Han et al. 2022). Nonetheless, the downstream pathways of *TTG2* during trichome development are unclear so far. The only direct target of *TTG2* identified is the single repeat MYB transcription factor *TRIPTYCHON* (*TRY*) (Hülkamp et al. 1994; Schellmann et al. 2002; Pesch et al. 2014). *TTG2* physically binds to the promoter of *TRY* to upregulate *TRY* expression (Pesch et al. 2014). The *try* mutant shows a cluster frequency and reduced trichome numbers that is similar to those in the *ttg2-1* mutant (Hülkamp et al. 1994; Johnson et al. 2002), suggesting *TTG2* serves as a regulator of *TRY* for trichome initiation and distribution. However, given the multiple trichome defects in *ttg2* mutants, it is interesting to consider the possibility that other cellular pathways coordinate with *TTG2* to modulate trichome development.

Genetic and pharmacological information have implicated the cooperative requirements of cortical microtubules (cMTs) and actin filaments (F-actin) cytoskeleton organization in defining trichome development (Smith and Oppenheimer 2005; Szymanski 2005; Sambade et al. 2014; Li et al. 2019). Mutations in genes involved in cMTs and F-actin assembling and dynamics often lead to aberrant branch numbers and shapes (Smith and Oppenheimer 2005; Tominaga-Wada et al. 2011; Li et al. 2019). Specifically, it has been suggested that microtubules establish the formation and spatial distribution of trichome branches whilst actin microfilaments elaborate and maintain the overall trichome branch shapes (Mathur et al. 1999; Szymanski 2005; Sambade et al. 2014; Li et al. 2019). During trichome branching, microtubules reorient from a transverse to a longitudinal direction with respect to the branch growth axis (Mathur and Chua 2000; Basu et al. 2005). Meanwhile, actin microfilaments assume an increasing degree of complexity from fine filaments to thick, longitudinally stretch cables during trichome formation (Mathur et al. 1999; Szymanski et al. 1999). In addition, around the time of branch initiation, an obvious microtubule-depleted zone (MDZ) at the very tip and a transverse aligned microtubule arrays (MT collar) toward the base of MDZ are formed in the apical part of the elongating trichome stalks and branches (Sambade et al. 2014; Tian et al. 2015; Yanagisawa et al. 2015; 2018). Moreover, it is showed that MDZ is colonized by tip-localized transverse actin filaments, which is considered to play substantial roles for trichome morphogenesis

(Sambade et al. 2014; Yanagisawa et al. 2015, 2018). *ZWICHEL* (*ZWI*) encodes a Kinesin-like Calmodulin Binding Protein (KCBP) (Reddy et al. 1996; Oppenheimer et al. 1997). *ZWI* mutation results in trichomes failed to branch properly, producing less-branched trichomes with shortened stalks and blunted branch ends (Hülkamp et al. 1994; Folkers et al. 1997; Oppenheimer et al. 1997; Reddy and Day 2000). Further studies demonstrated that *ZWI* is part kinesin and part myosin (Reddy et al. 1996; Reddy and Reddy 1999) and the N-terminus MyTH4 domain and FERM domain of *ZWI* could physically bind to MTs and F-actin in vitro, respectively (Narasimhulu and Reddy 1998; Tian et al. 2015), implying *ZWI* may link and integrate microtubule and actin cytoskeleton for trichome cell shaping. However, deletion of these 2 domains has minor effects on the trichome morphologies, only inducing a slight increase of trichome branch numbers (Tian et al. 2015).

The *DISTORTED* (*DIS*) group genes encode subunits of the actin-related protein (ARP)2/3 and suppressor of cyclic AMP repressor (SCAR)/Wiskott–Aldrich syndrome protein family verprolin homologous protein (WAVE) complexes (Schwab et al. 2003; Szymanski 2005; Li et al. 2019), and loss-of-function of which result in fascinating “distorted” trichomes with alterations in the organization and/or density of F-actin in expanding trichomes (Hülkamp et al. 1994; Szymanski et al. 1999; Le et al. 2003; Li et al. 2004; Mathur et al. 2003a, 2003b; Schwab et al. 2003; Basu et al. 2004, 2005, 2008; Deeks et al. 2004; El-Assal et al. 2004a; Saedler et al. 2004a, 2004b; El-Din El-Assal et al. 2004b; Zhang et al. 2005a, 2005b; Zhang et al. 2008; Jörgens et al. 2010; Yanagisawa et al. 2015, 2018). *HSPC300* is a conserved 8 kDa human protein and participates in ARP2/3 activation through interacting with WAVE proteins (Stovold et al. 2005). *BRICK1* (*BRK1*) is the maize (*Zea mays* L.) homolog of *HSPC300* and loss-of-function mutations result in the absence of epidermal pavement cell lobes formation and short and swollen leaf hairs (Gallagher and Smith 2000; Frank and Smith 2002). These defects were associated with loss of localized cortical F-actin enrichment, implying a role for *BRK1* in promoting actin polymerization (Gallagher and Smith 2000; Frank and Smith 2002). Likewise, the Arabidopsis *brk1* mutant displays a strongly distorted trichome phenotype accompanied by the alteration in F-actin organization in trichome branches as well (Djakovic et al. 2006; Le et al. 2006). *BRK1* is considered to be essential for the SCAR/WAVE-ARP2/3 pathway in plants by selectively stabilizing SCAR1 and SCAR2 proteins (Djakovic et al. 2006; Le et al. 2006; Dyachok et al. 2011). The localization experiments revealed that *BRK1* is enriched to the apex of young trichome branches (Dyachok et al. 2008; Yanagisawa et al. 2018), and such a specific localization may reflect the important role of *BRK1* in onset of cell polarity because fused *BRK1*-YFP also accumulates at the apex of tip growing cells (Perroud and Quatrano 2008; Chin et al. 2021). It has been reported that the DOCK family guanine nucleotide exchange factor (GEF) *SPIKE1* (*SPK1*) is required for actin-dependent cell morphogenesis and the tip enrichment of *BRK1* in

developing trichome branches (Basu et al. 2008; Yanagisawa et al. 2018). In *spk1* mutant, majority of trichome branches have no BRK1 signals or show mislocalized signals at the trichome apex. However, whether there are other factors responsible for regulating BRK1 activity are still interesting.

In this study, we report that the WRKY transcription factor TTG2 could directly binds and regulates the expression of BRK1 during trichome morphogenesis. We found that a mutant allele of TTG2, *ttg2-6*, produces conspicuous distorted trichomes which are reminiscent of *brk1* mutants. Genetic and molecular analyses indicated that BRK1 functions downstream of TTG2. Taken together, our results show a connection between TTG2 and cytoskeletal regulators, revealing a previous unknown pathway in trichome development as well as in BRK1 activity regulation.

Results

abt4-1 mutant displays pleiotropic trichome developmental defects

In our continuous effort to uncover unidentified molecular mechanisms involved in plant cell morphogenesis, we performed genetic screening for trichome phenotypes, and a unique recessive trichome mutant, designated as *aberrantly branched trichome 4-1* (*abt4-1*) was isolated (Supplementary Fig. S1A). The overall growth and development of *abt4-1* were not substantially different from that of wild type (WT), but it exhibited striking pleiotropic trichome defects (Fig. 1, A to G; Supplementary Fig. S1, B and C). Under our growth conditions, the trichomes of WT plants are predominately 3- or 4-branched (approximately 71% 3-branched and 28% 4-branched in the 3rd rosette leaves, respectively), while less or more branched trichomes are rare (Fig. 1, A, C, D, and H). Moreover, WT trichomes are precisely distributed in leaves, and clustered trichomes are scarcely observed (Fig. 1, A and J). In contrast, *abt4-1* mutants displayed trichome developmental defects in multiple aspects. First, *abt4-1* trichomes were variable in branch numbers, ranging from 1 to 7-branched, and even 9-branched trichomes were observed (Fig. 1, E to G and H). Second, some of the trichomes in *abt4-1* showed twisted and swollen branches (Fig. 1, E and G), resembling those of dis-group mutants (Hülkamp et al. 1994; Schwab et al. 2003; Smith and Oppenheimer 2005; Szymanski 2005; Li et al. 2019). Third, *abt4-1* mutants also exhibited trichome distribution defects, with ~5% of trichomes arising closely to another and forming trichome clusters (Fig. 1, E and J). Fourth, trichome density was apparently decreased in *abt4-1* plants (approximately 2.9 trichomes per mm² in *abt4-1* versus 3.6 trichomes per mm² in WT) (Fig. 1L), implying that trichome initiation was also impaired. Finally, some *abt4-1* trichomes lacked surface papillae, and appeared dark gray when viewed under scanning electron microscopy (Fig. 1B), indicating a defective trichome maturation process. Similar trichome developmental differences were also observed in the 4th rosette leaves between the WT and the *abt4-1* mutant (Fig. 1, I, K, and M). Taken

together, these phenotypic observations suggest that ABT4 serves as a crucial genetic factor in controlling multiple aspects of trichome development.

abt4-1 is a recently discovered mutant allele of TTG2

To characterize the molecular identity of the ABT4, we cloned the ABT4 locus through map-base cloning and nucleotide sequencing, and a G to A substitution in the 4th exon of AT2G37260 gene was detected in *abt4-1* (Fig. 2A; Supplementary Fig. S2). AT2G37260 encodes the key regulator of trichome development, TTG2 (Johnson et al. 2002). Theoretically, this mutation would convert the corresponding codon from cysteine to tyrosine (C379Y) that is located in the second CCHH zinc finger motif in TTG2 (Fig. 2B), which is well conserved in TTG2 homologs and is assumed to take part in target binding (Johnson et al. 2002; Li et al. 2015). To determine whether ABT4 is indeed represented by TTG2, we performed genetic complementation experiments. After expressing the coding region of TTG2 driven by its native promoter (*pTTG2:TTG2*) in the *abt4-1*, we identified multiple independent *abt4-1 pTTG2:TTG2* transgenic lines (46 in total), and 2 of them were used for detailed phenotypic analyses. These plants produced WT-like trichome phenotypes including morphology, distribution, and trichome density (Fig. 2F). Consistently, they show relative higher TTG2 expression levels compared to that in *abt4-1* (Fig. 2G). Quantitative measurements confirmed the phenotypic observations (Fig. 2, C to E). These results indicate that in planta expression of TTG2 can rescue the trichome developmental defects of *abt4-1*, and ABT4 is TTG2. Therefore, *abt4-1* was renamed as *ttg2-6* based on earlier nomenclature.

Since in previous reports describing the *ttg2* mutants in the *Ler* background (*ttg2-1* and *ttg2-2*), 1 of the major defects is to reduce or eliminate branching (Johnson et al. 2002), which is in strikingly contrast to the hyper-branched trichomes observed in *abt4-1*. To examine this issue, we identified 2 independent T-DNA insertion lines of TTG2 in *Col-0* background, *Salk_148838* (*ttg2-3*) and *Salk_206852* (*ttg2-7*) (Fig. 3A). These 2 mutations likely represent null alleles of TTG2 because we did not detect any TTG2 transcripts in both *ttg2-3* and *ttg2-7* (Fig. 3F). Homozygous *ttg2-3* and *ttg2-7* mutants showed similar defects as those in *abt4-1*, including reduced trichome numbers, and clustered and distorted trichomes (Fig. 3, B, D, and E). However, unlike the variable trichome branch numbers in *ttg2-6*, the majority of trichomes were 1- or 2-branched in *ttg2-3* and *ttg2-7* (Fig. 3, B and C). The F1 plants of crosses between *ttg2-6* and *ttg2-3*, as well as *ttg2-6* and *ttg2-7*, were defective in trichome numbers, distributions, and branch extensions (Fig. 3, B, D, and E), indicating that both *ttg2-3* and *ttg2-7* failed to complement *ttg2-6* for these defects. Nevertheless, the trichome branching pattern of the F1 plants resembled that of *ttg2-6* (Fig. 3, B and C), suggesting that *ttg2-6* is epistatic to *ttg2-3* and *ttg2-7* with regard to the degree of trichome branching. Among the mutant alleles of TTG2 reported so far (Johnson et al. 2002; Ishida et al.

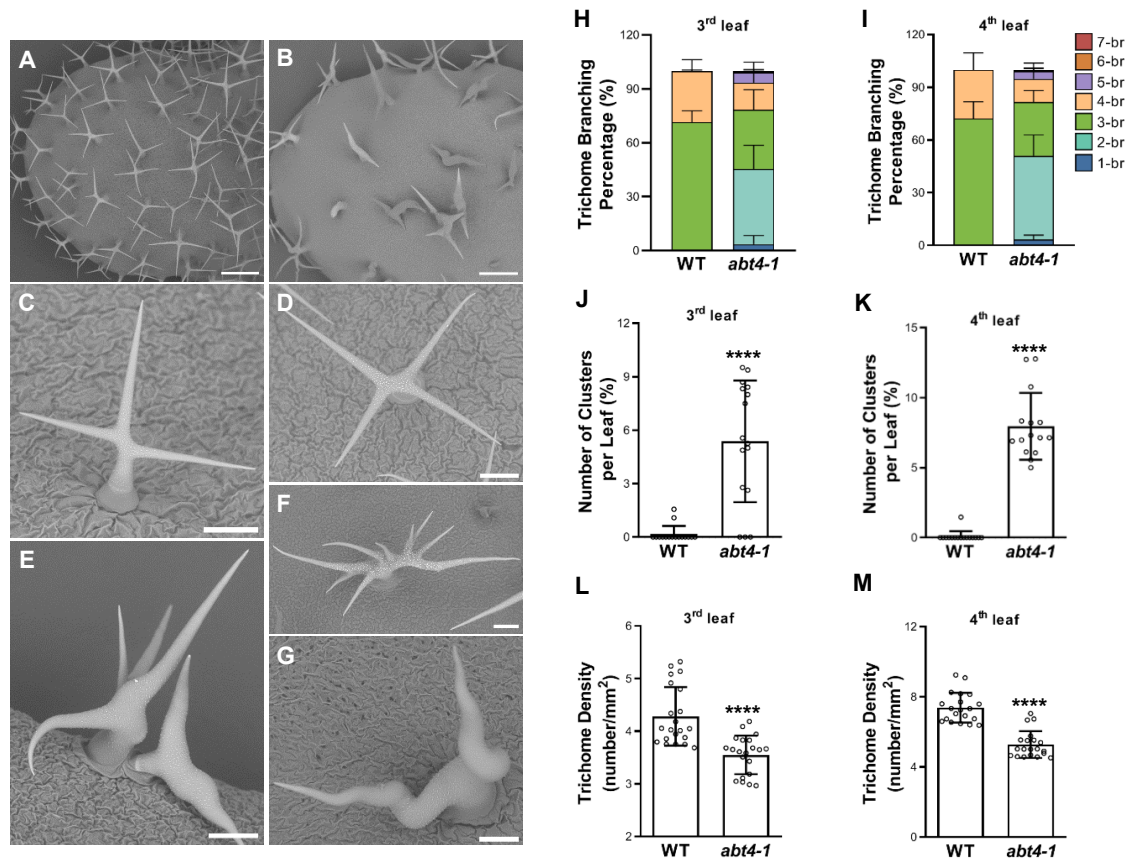


Figure 1. Characterization of trichome phenotypes from the wild type (WT) and *abt4-1* mutant plants. **A to G**) Representative trichomes on the fifth rosette leaves of 3-wk-old WT (*Col-0*) **A, C, and D**) and *abt4-1* **B and E to G**). For **A and B**), bars = 400 μm , for **C to G**), bars = 100 μm . **H to M**) Quantification of the trichome branch numbers **H and I**), cluster numbers **J and K**), and trichome density **L and M**) of in WT and *abt4-1* on the third **H, J, and L**) and fourth rosette leaves **I, K, and M**), respectively. 1/2/3/4/5/6/7-br for one/two/three/four/five/six/seven-branched trichomes, respectively. At least 15 independent plants for each genotype were used for statistical analyses. Data are shown as means \pm SD. **** $P \leq 0.0001$ by the Student's *t*-test.

2007), only *tig2-6* displayed hyper-branched trichomes. Thus, *tig2-6* is likely to represent a unique allele of *TTG2*.

tig2-6 displays altered cytoskeletal configurations in trichome cells

Given the highly similar trichome morphologies of the *tig2-6* mutant and those of loss-of-function mutants of genes encoding microtubule- and actin-associated proteins (Szymanski 2005; Ishida et al. 2007; Tominaga-wada et al. 2011; Li et al. 2019), we reasoned that *TTG2* may regulate trichome development through the cytoskeletons. To address this issue, we first examined the cMTs and F-actin configurations in *tig2-6* trichomes. Because the detection of cytoskeleton organization should be focused on the stages of development at which the mutant phenotypes are first apparent, for a first step, we quantitatively measured the *tig2-6* trichome phenotypes at different developmental stages according to Szymanski et al. (1999) and Szymanski (2001). Overall, trichomes in *tig2-6* were larger in size than those in the WT (Fig. 4A; Supplementary Fig. S3A). Statistical

data showed that *tig2-6* trichomes display differences from the WT as early as Stage 1. Trichomes diameters in *tig2-6* at Stage 1 were remarkably wider than those in the WT ($32.62 \pm 10.79 \mu\text{m}$ in *tig2-6* versus $16.90 \pm 2.63 \mu\text{m}$ in WT) (Fig. 4, A and B). In later stages, *tig2-6* trichomes consistently showed apparently wider stalks compared those in the WT (Fig. 4, A and C to F; Supplementary Fig. S3B), indicating decreased polar growth in *tig2-6* trichomes. Similar results were obtained in branch phenotypes at different developmental stages; *tig2-6* exhibited remarkable swollen branches compared those in the WT (Fig. 4, G and H; Supplementary Fig. S3C).

Based on the morphological analyses, we compared the cMTs and F-actin arrangements in the WT trichomes to those in *tig2-6* at various developmental stages. By visualizing cMTs with TUB6-GFP in living cells, we found that both WT and *tig2-6* trichomes display randomly oriented microtubule during Stage 1 (Supplementary Fig. S4, A and G), which is consistent with the radially expanding nature of Stage 1 trichome cell (Szymanski et al. 1999, 2001). With the protruding from the leaf plane, transverse organized microtubule

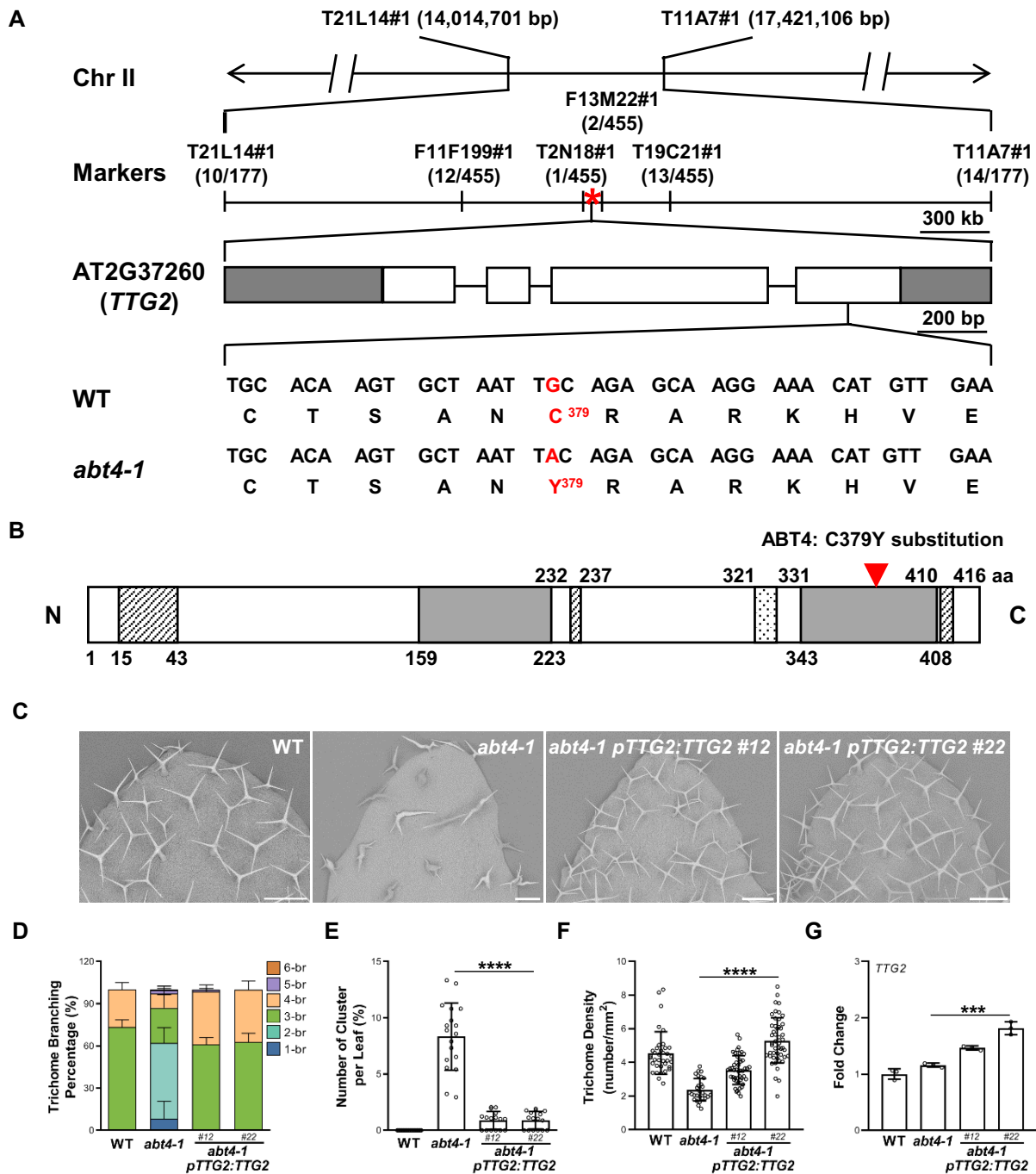


Figure 2. Cloning and genetic complementation of *ABT4*. **A**) Map-based cloning of *abt4-1*. The *ABT4* locus was preliminarily located between markers T21L14 and T11A7 on chromosome II. Fine-mapping restricted the locus within a region between T2N18 and F13M22. The numbers of genetic recombinants are shown under each marker. The asterisk indicates the position of the *TTG2* gene, AT2G37260. In the schematic gene structure, white rectangles and solid lines represent the exons and introns, respectively. The 5' and 3' untranslated regions are shown as gray rectangles. The highlighted nucleotide below the gene model indicates the exact position of the mutation site. **B**) *TTG2* protein structure and deduced mutation in the amino acid sequence. The 2 WRKY domains are indicated as shaded boxes. The putative Ser/Thr-rich activation domains and a possible nuclear localization signal are shown as slash lined and dotted boxes, respectively. The arrowhead shows the position of the C379Y mutation in *ABT4* located in the second WRKY domain. **C**) Trichome branching phenotypes of WT (*Col-0*), *abt4-1* and the genetic complementation lines (*abt4-1 pTTG2:TTG2 #12* and *abt4-1 pTTG2:TTG2 #22*). Bars = 100 μ m. **D** to **F**) Quantification of trichome branch numbers **D**), cluster numbers **E**), and trichome density **F**) on the fourth rosette leaves of plants shown in **C**). 1/2/3/4/5/6-br for one/two/three/four/five/six-branched trichomes, respectively. At least 15 independent plants for each genotype were used for statistical analyses. Data are presented as mean \pm SD. **** $P \leq 0.0001$ by the Student's *t*-test. **G**) RT-qPCR analysis of *TTG2* transcripts levels in WT, *abt4-1* and the complementation lines. Data are shown as means \pm SD of 3 biological replicates. *** $P \leq 0.001$ and **** $P \leq 0.0001$ by the Student's *t*-test.

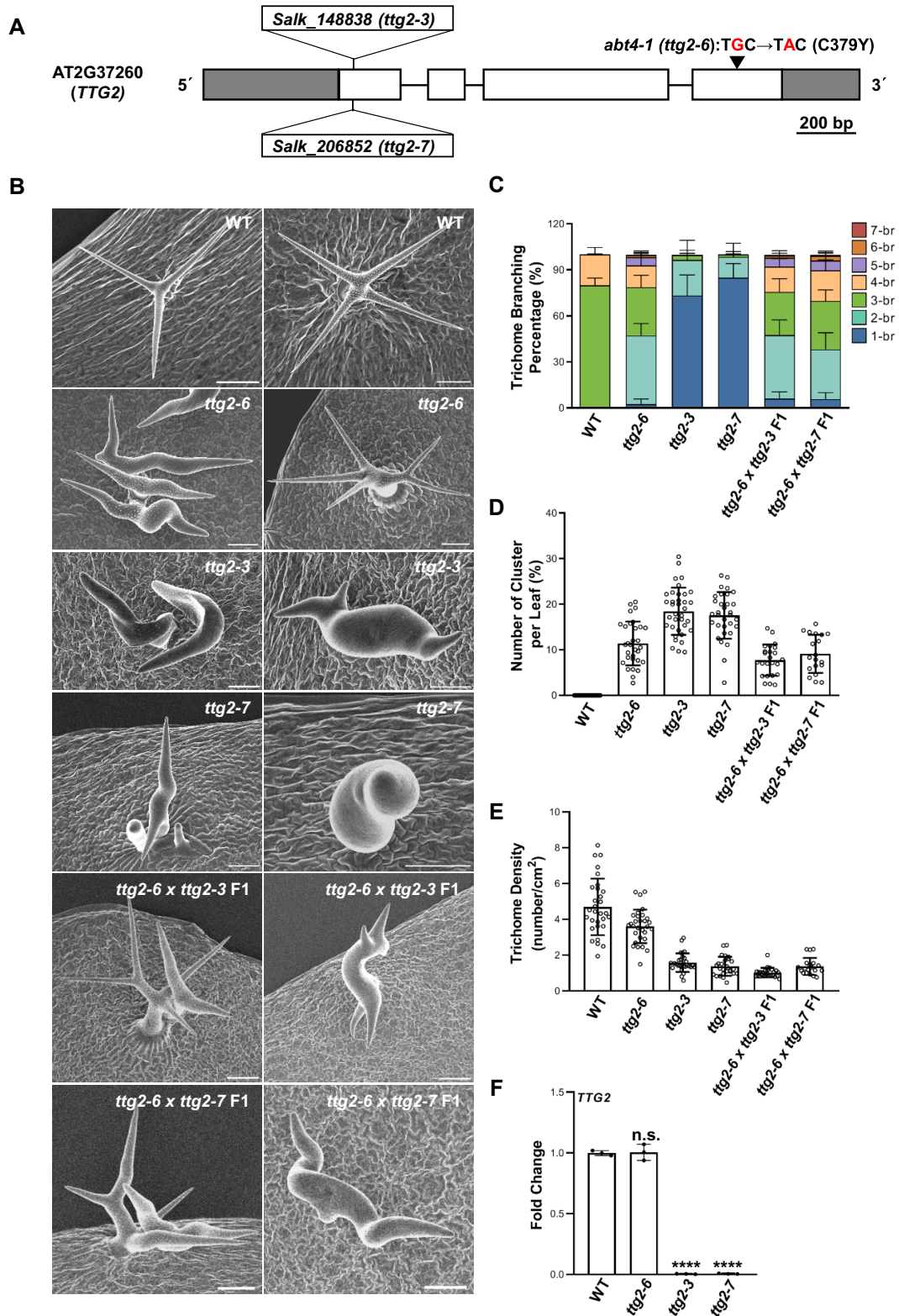


Figure 3. Trichome phenotypes of various *TTG2* alleles. **A**) Schematic representation of the mutation sites in *ttg2-6*, *ttg2-3* (*Salk_148838*), and *ttg2-7* (*Salk_206852*). **B**) Representative trichomes on the fifth rosette leaves of WT (*Col-0*), *ttg2-6*, *ttg2-3*, and *ttg2-7*. Bars = 100 μ m. **C to E**) Quantification of trichome branch numbers **C**), cluster numbers **D**), and trichome density **E**) of WT, *ttg2-6*, *ttg2-3*, *ttg2-7*, *ttg2-6* \times *ttg2-3* F1, and *ttg2-6* \times *ttg2-7* F1. Thirty independent plants for each genotype were used for statistical analyses. Data were shown as means \pm SD. 1/2/3/4/5/6/7-br for one/two/three/four/five/six/seven-branched trichomes, respectively. **F**) The relative expression levels of *TTG2* in different *TTG2* alleles measured by RT-qPCR. Data are shown as means \pm SD of 3 biological replicates. n.s., no significance, **** $P \leq 0.0001$ by the Student's *t*-test.

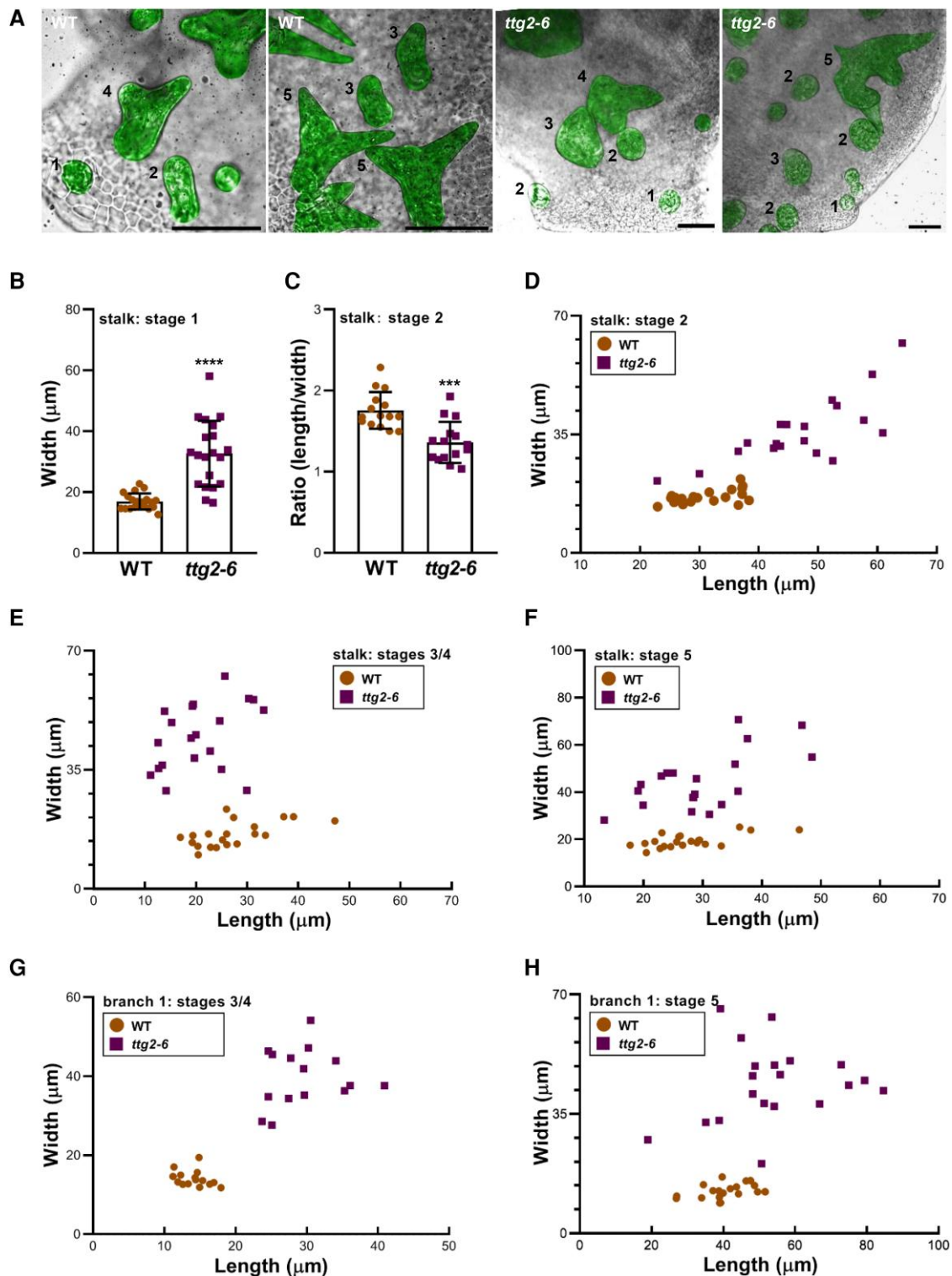


Figure 4. Quantitative examination of trichome phenotypes in *ttg2-6* at major developmental stages. **A**) Representative trichomes at appropriate developmental stages. Numbers to each labeled trichome indicate its developmental stages. Bars = 50 μm . WT refers to *Col-0*. **B**) Measurements of trichome width at Stage 1. **C to H**) Measurements of stalk length and width of trichome stalk and Branch 1 at Stage 2 (**C, D**), Stage 3/4 (**E, G**), and Stage 5 (**F, H**). Stage 1 trichomes used for measurement were radially expanded cells within the epidermis or with a height less than 10 μm . At Stage 2, stalk length was defined as distance from the leaf surface to the cell tip, while at other stages, stalk length was the distance from the leaf surface to the lowest edge of the first branch. Trichomes with branches between 10 and 15 μm in length were categorized as Stage 3/4 and those between 16 and 50 μm in length were categorized as Stage 4/5 in WT. Because of the larger size in *ttg2-6*, trichomes for appropriate stages were classified according to morphological observation. The width of branch was measured at the branch base. For **B and C**) 20 independent cells for each genotype were used for statistical analyses. Data are shown as means \pm SD. *** $P \leq 0.001$ and **** $P \leq 0.0001$ by the Student's *t*-test.

collar began to form at the apex of the WT stalks and aligned microtubule arrays appeared toward the base of stalks (Supplementary Fig. S4B). By comparison, *ttg2-6* stalks still displayed disorganized microtubules, and spread from the apex to the base (Supplementary Fig. S4H). At late Stage 2, the microtubule collar at the apex and the aligned microtubule arrays at the base of stalks became remarkable in WT (Supplementary Fig. S4C). Meanwhile, the regions with sparse microtubule meshworks at the extreme apex were also observed. Similar to those observed at late Stage 1, microtubules in *ttg2-6* stalks were densely distributed at the extremely tip and randomly oriented along the growth axes (Supplementary Fig. S4I). At Stage 3/4 branches, both WT and *ttg2-6* branches showed clear transverse orientation of microtubules relative to the long axis, but the transverse aligned microtubules arrays diffused toward the base of branches in *ttg2-6* (Supplementary Fig. S4, D and J). Previous studies showed that the beginning of reorientation of microtubules from a transverse to a helical or longitudinal arrangement is first detected in branches that are about 30 μm in length (Basu et al. 2005). In consistent, we also observed such a transition in WT branches at Stage 5 (Supplementary Fig. S4E). However, transverse oriented microtubules persisted in *ttg2-6* trichome branches (Supplementary Fig. S4K). In the mature trichomes, almost all of the WT branches had highly longitudinal aligned microtubules along the elongation axes of the branches, whereas similar staged *ttg2-6* branches retained transverse microtubule organization (Supplementary Fig. S4, F and L).

The actin cytoskeleton was assayed according to Le et al. (2003) and Chang et al. (2019) by probing ABD2-GFP (Sheahan et al. 2004; Basu et al. 2005). We found that actin in both WT and *ttg2-6* trichomes show diffuse actin cytoskeleton during Stage 1, which is consistent to previous reports (Mathur et al. 1999; Szymanski et al. 1999). To reveal the early stages at which actin organization exhibit abnormality in *ttg2-6* trichomes, we then assayed the actin-based phenotypes at Stage 2, and a disorganization of actin arrays was revealed in *ttg2-6*. As reported before (Szymanski et al. 1999), actin strands in WT stalks were loosely arranged along the growth axis and not limited to the cortex, while diffuse actin filaments appeared at the apex of the stalks (Fig. 5A). In contrast, *ttg2-6* failed to generate organized actin arrays, showing disordered and discontinuous actin filaments throughout the stalks (Fig. 5A). Because it has been shown that actin organization is important to trichome cell morphogenesis at or near the transition from Stage 3 to Stage 4 (Szymanski et al. 1999), we examined the actin arrangement in branches during Stages 3 and 4 as well. WT trichome branches at these stages showed densely cytoplasmic actin. The intensity and complexity of the signal associated with initiating branches, while actin strands were aligned with the future long axis of the developing branch (Fig. 5A). Similar staged *ttg2-6* branches still showed randomly oriented actin filaments, without obvious ordered organized actin (Fig. 5A). A quantitative measurement of the relative amount of cytoplasmic

actin and average actin angles was consistent with the localization data. WT stalks showed higher intensity ratio (core actin/total cytoplasmic actin) than those in *ttg2-6* (Fig. 5, B and C). Statistical analyses on angles and anisotropy of total actin filaments also revealed a higher ordered organization of F-actin in WT stalks. At Stage 2, the major proportion of actin filaments in WT stalks were arranged from 0° to 15° relative of growth axis and with an anisotropy in average of 0.12 ± 0.07 (Fig. 5, C and D). By comparison, angles of the actin filaments in *ttg2-6* stalks were scattered from 0° to 90°, and the mean value of the anisotropy was 0.06 ± 0.03 (Fig. 5, C and D). At Stage 3/4, although WT Branch 1 showed higher actin intensity ration than those in *ttg2-6*, the actin anisotropy was undistinguishable (Fig. 5, B and C). These might be due to the intensity and complexity actin signals in initiating branches, because we observed apparent divergence at the later developmental stages with the extension of branches (Fig. 5, B to D).

TTG2 interacts genetically with BRK1 and promotes BRK1 expression

The striking effects of *TTG2* on cMTs and F-actin organization during trichome development raised the possibility that *TTG2* may influence cytoskeleton organization through targeting factors associating with cMTs and F-actin biosynthesis or dynamics. Therefore, for a first step, we constructed a series of double mutants by crossing *ttg2-6* with mutants of genes encoding proteins involved in cMTs dynamics and SCAR/WAVE-ARP2/3 subunits, respectively, to perform genetic analyses (Supplementary Figs. S5 to S8). During the investigating of trichome phenotypes of the double mutants, we found that *TTG2* interacts genetically with *BRK1*. *BRK1* mutations result in swollen stalks and aborted branches (Gallagher and Smith 2000; Frank and Smith 2002; Djakovic et al. 2006; Le et al. 2006). In *ttg2-6 brk1-1* double mutants, both the overall plant phenotypes and the trichome morphologies of mature trichomes were very similar to the *brk1-1* single mutant (Fig. 6A; Supplementary Fig. S9A), indicating *brk1* was probably epistatic to *ttg2* in regulating stalk and branch extension. To verify the genetic interaction between *TTG2* and *BRK1*, we quantitatively assayed trichome morphologies of *brk1-1* mutant at different developmental stages. Although previous reports indicated that trichome morphological changes in WAVE and ARP2/3 subunit mutants occur during Stages 3 and 4 (Szymanski et al. 1999; Basu et al. 2004, 2005; El-Assal et al. 2004; Zhang et al. 2008), our data showed that *brk1-1* trichomes frequently had swollen stalks compared with the WT as early as Stage 2 (Fig. 6, E to G), with the ratio of length to width 1.54 ± 0.19 compared to that of 1.98 ± 0.26 in the WT. These might be responsible for the specific genetic interaction between *TTG2* and *BRK1*. Investigation of actin cytoskeleton arrangement revealed the coincidence with the morphological observations. Similar to those in *ttg2-6*, *brk1-1* trichomes showed lower actin intensity ratio and organization at Stage 2 stalks (Fig. 7, A

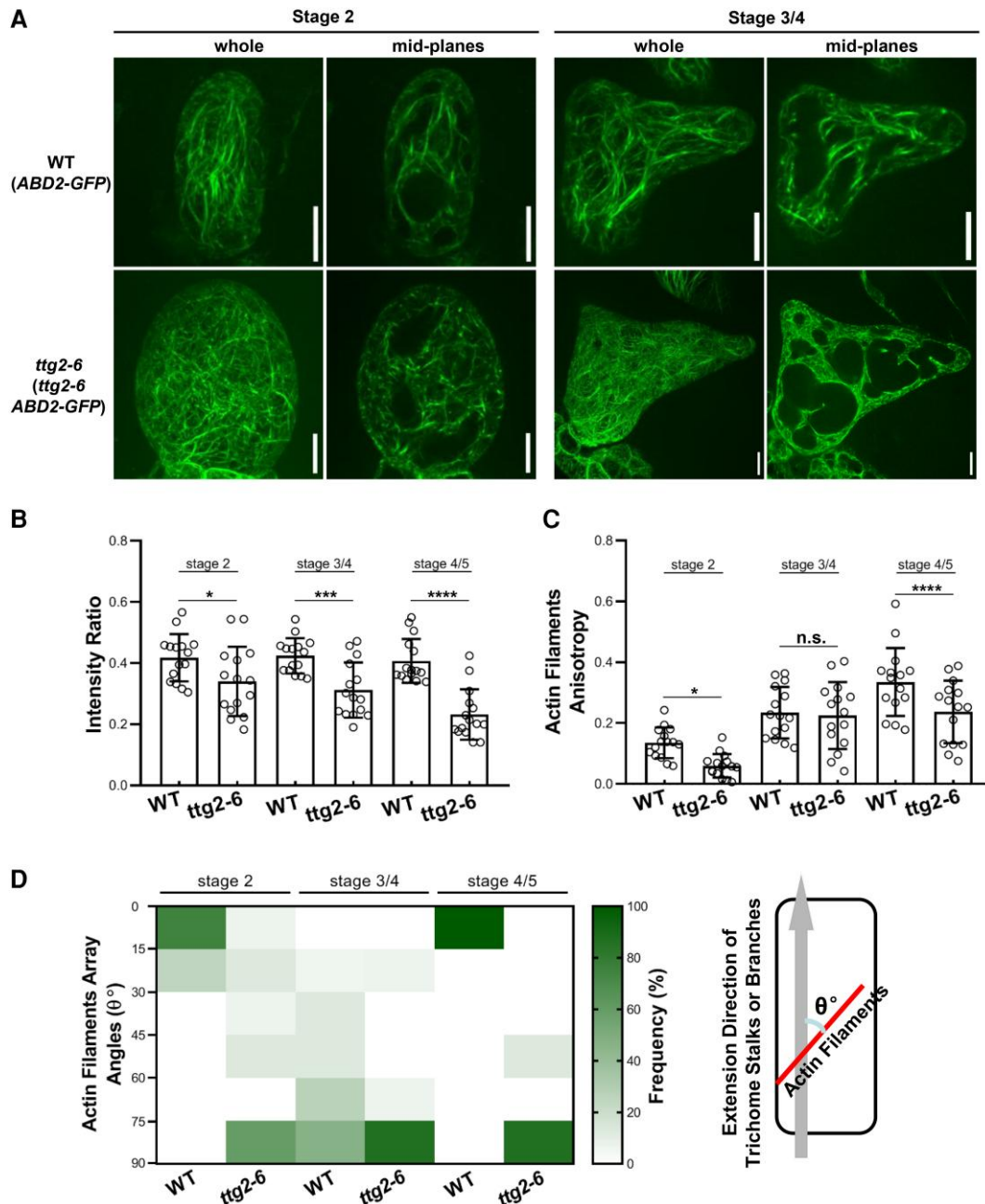


Figure 5. Localization and quantification of actin filaments in *ttg2-6* Stage 2 and Stage 3/4 trichomes. **A**) Typical actin organization visualized using ABD2-GFP under spinning disk confocal microscopy at Stage 2 (left 2 panels) and Stage 3/4 (right 2 panels) trichomes in WT (ABD2-GFP) and *ttg2-6* ABD2-GFP mutant. Whole actin signals were the maximum projections of confocal image stacks that include the entire cell and actin signals in mid-planes were the maximum projections of confocal images of the core cytoplasm that didn't include outer cortical actin signals (within $2.5 \mu\text{m}$ of plasma membrane). Bars = $10 \mu\text{m}$. **B**) Quantification of the ratio of core cytoplasmic actin signals to total actin signals in stalks at Stage 2 and in Branch 1 at Stage 3/4 and Stage 4/5 trichomes. The signals were calculated with Fiji ImageJ software. At least 15 independent trichome cells for each genotype were used for statistical analyses. **C and D**) Quantification of actin arrangements with respect to actin anisotropy **C**) and angles **D**). The actin anisotropy and angles were evaluated with ImageJ plug-in FibrilTool described by Boudaoud et al. (2014) and Chang et al. (2019). The anisotropy score 0 is defined for purely isotropic arrays (no order), and 1 is defined for purely anisotropic arrays (perfectly order). Angles of actin filaments that are parallel to the stalk and branch extension directions are defined as 0° , whereas the angles of those perpendicular to the growth axis are defined as 90° . About 20 independent trichomes were used for measurements. Data were expressed as means \pm SD. n.s., no significance, $*P \leq 0.1$, $***P \leq 0.001$, and $****P \leq 0.0001$ by the Student's *t*-test. For **D**), actin angles in average from 20 independent trichomes were divided into 6 intervals mandatorily (0° to 15° , 15° to 30° , 30° to 45° , 45° to 60° , 60° to 75° , 75° to 90°). The frequency in each interval was calculated by dividing the number of trichomes with the corresponding actin angles in each interval by the total number of trichomes, and then displaying as a heatmap with GraphPad Prism software.

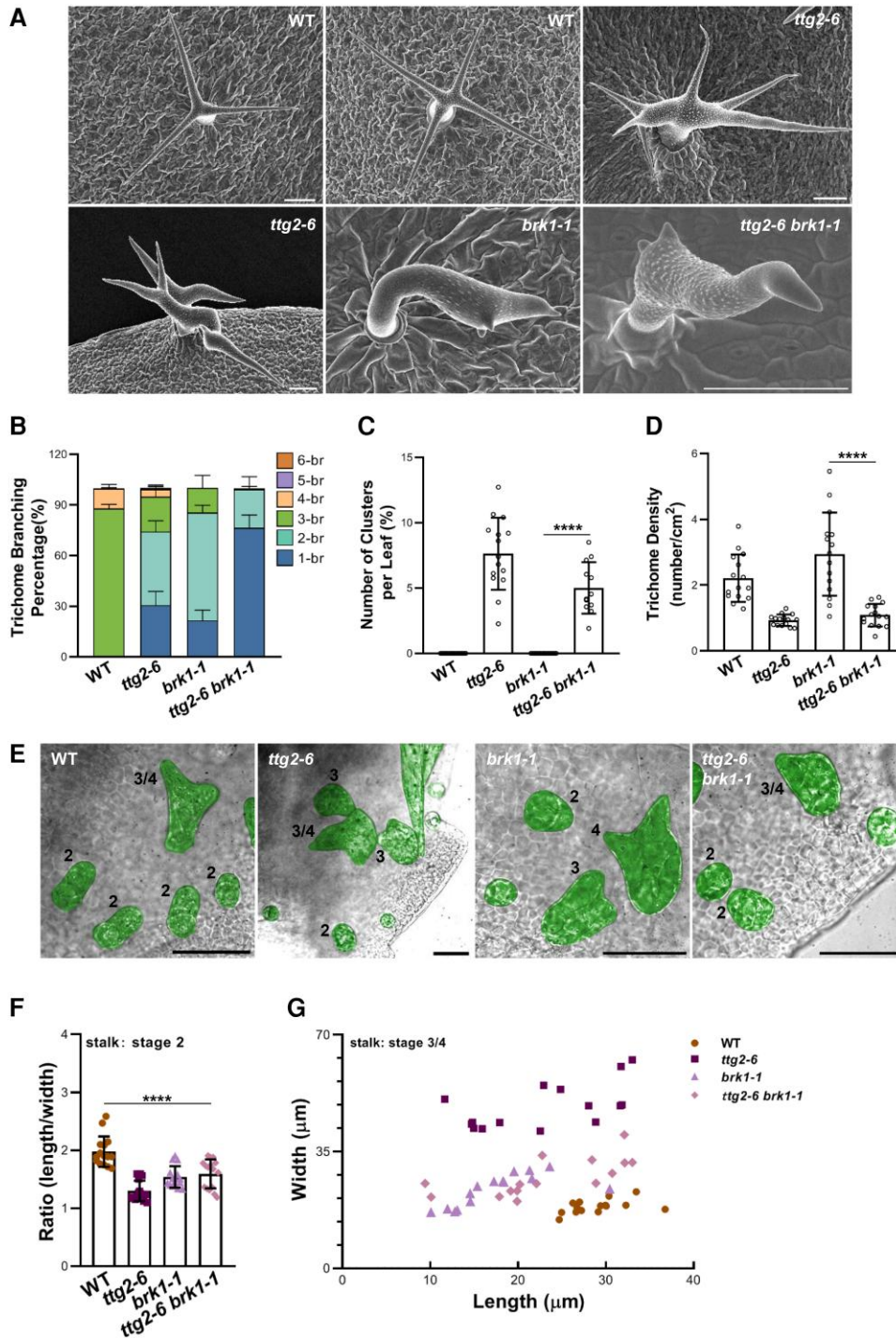


Figure 6. Trichome phenotypes of *ttg2-6 brk1-1* double mutants. **A)** Representative trichomes on the fifth rosette leaves of WT (*Col-0*), *ttg2-6*, *brk1-1*, and *ttg2-6 brk1-1*. Bars = 100 μm. **B to D)** Quantification of trichome branch numbers **B)**, cluster numbers **C)**, and trichome density **D)** of the plants shown in panel **A)**. **E)** Representative trichomes at certain developmental stages in indicated genetic background. Numbers to each labeled trichome show its developmental stage. Bars = 50 μm. **F and G)** Quantitative measurements of stalk dimensions at Stage 2 **F)** and Stage 3/4 **G)** trichomes. For **B to D, F, and G)**, 15 independent plants and trichome cells for each genotype were used for statistical analyses. Data are shown as means ± SD. **** $P \leq 0.0001$ by the Student's *t*-test.

to **C)**. We also analyzed the morphological phenotypes at Stage 3/4. *brk1-1* trichomes still showed swollen stalks (with width of 23.64 ± 4.72 μm in average in *brk1-1* versus 18.52 ± 2.04 μm in WT), while the width of the Branch 1

was undistinguished (**Fig. 6, F and H**), only with remarkably reduced branch length. Actin arrangements in *brk1-1* branches showed severer abnormality compared to those in *ttg2-6* at the Stage 3/4 trichomes (**Fig. 7, A to D**), whereas

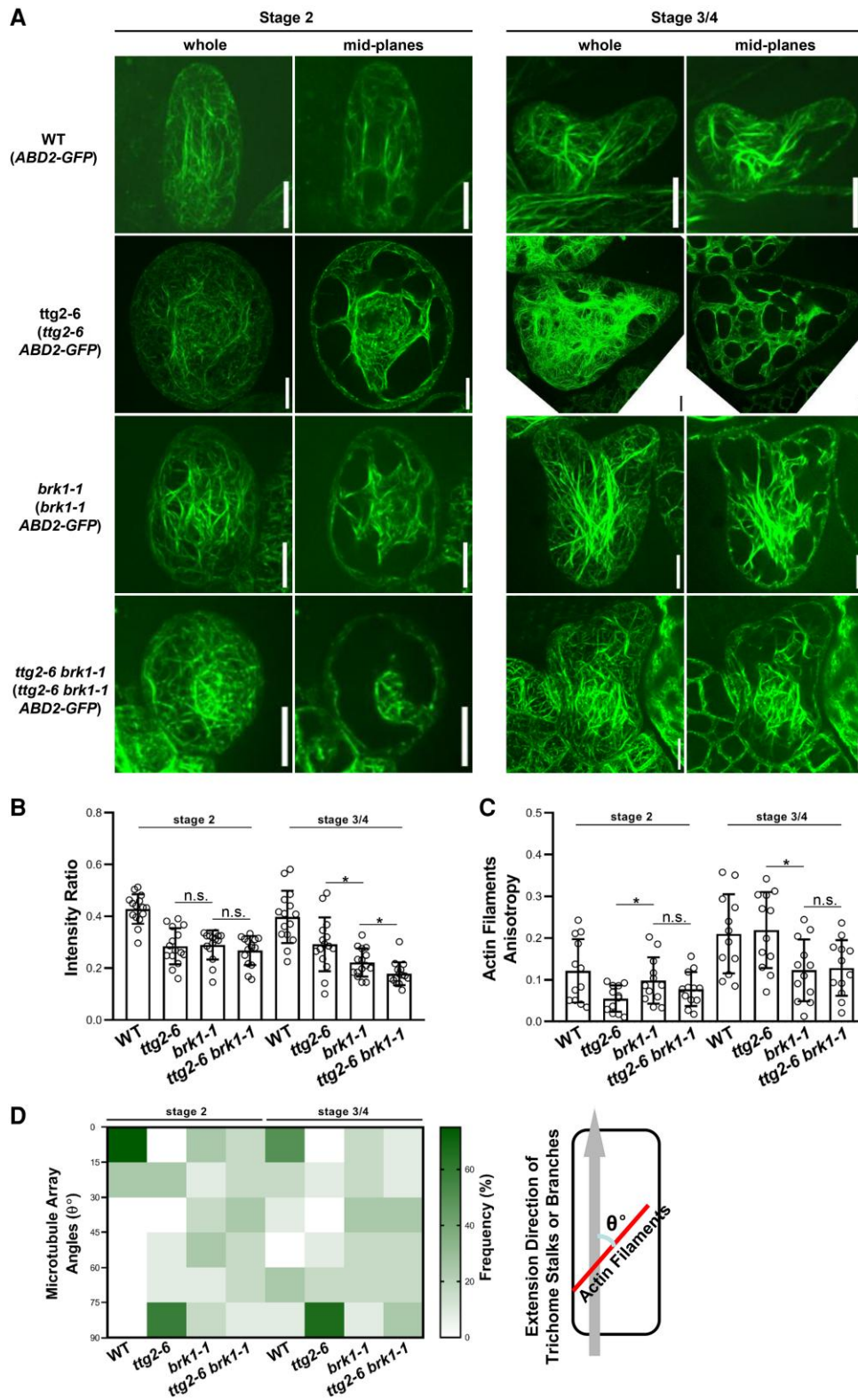


Figure 7. F-actin organization in *ttg2-6 brk1-1* double mutants. **A)** Typical F-actin organization probed with ABD2-GFP in the stalks at Stage 2 (left 2 panels) and Branch 1 at Stage 3/4 trichomes (right 2 panels) in different genotypes. Bars = 10 μ m. WT refers to ABD2-GFP. **B)** Quantification of the intensity ratio of core cytoplasmic actin signals to total actin signals in stalks at Stage 2 and in Branch 1 at Stage 3/4 trichomes. **C and D)** Measurements of actin arrangements with respect to actin anisotropy **C)** and angles **D)**. Similar parameters and methods as those indicated in Fig. 6 are employed. For **B to D)**, at least 15 independent trichome cells were used for statistical analyses. Data are shown as means \pm SD for **B and C)**. n.s., no significance, $*P \leq 0.1$ by the Student's *t*-test.

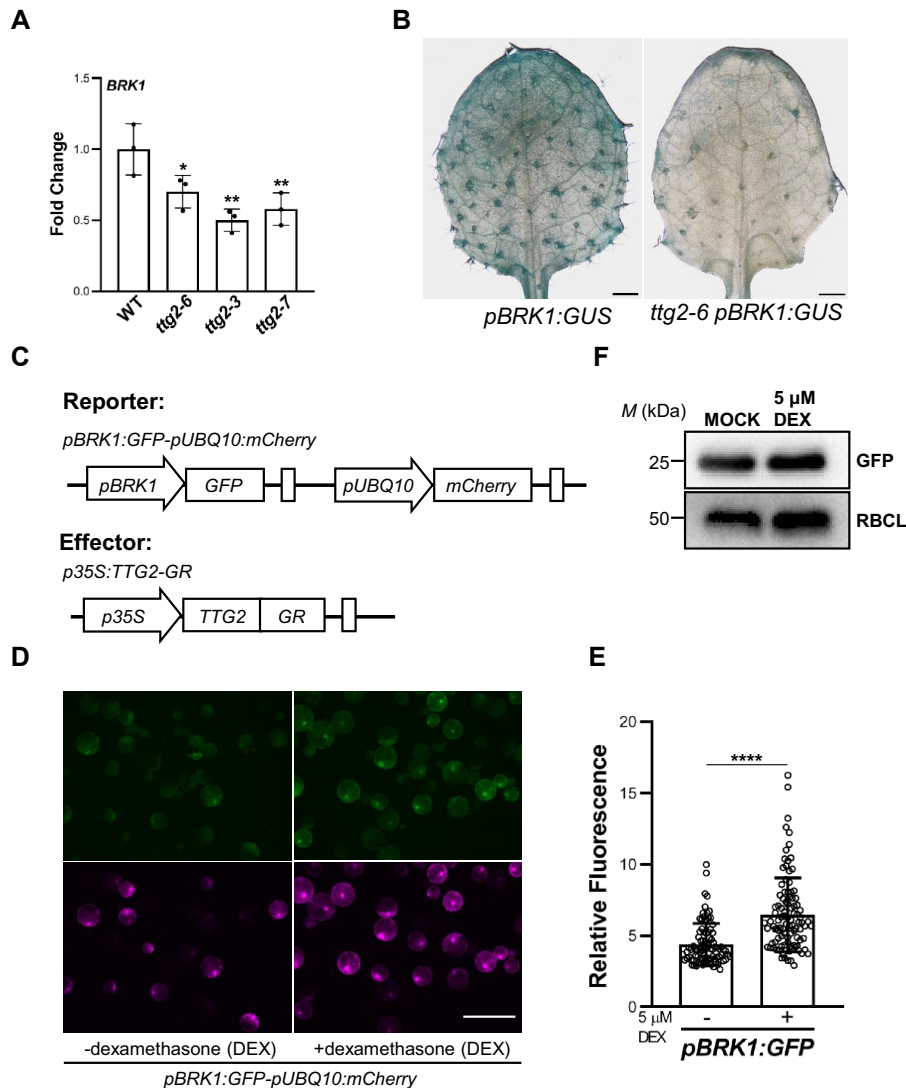


Figure 8. *TTG2* modulates *BRK1* expression. **A**) RT-qPCR analyses of the relative expression levels of *BRK1* in *ttg2* mutants. Data are shown as means \pm SD of 3 biological replicates. ****** $P \leq 0.01$ by the Student's *t*-test. WT refers to *Col-0*. **B**) The expression patterns of *pBRK1:GUS* in the WT (*Col-0*) and *ttg2-6*. *BRK1* expression was indicated by *GUS* expression from the fusion of the *GUS* reporter gene to the 5' regulatory region of *BRK1*. Bars = 500 μ m. **C to F**) Protoplast-based effector/reporter assays. **C**) Diagrams of the reporter and effector vectors. **D**) Representative GFP fluorescence signals in the protoplast cells when effector vector *p35S:TTG2-GR* was co-expressed with reporter vector *pBRK1:GFP-pUBQ10:mCherry* in WT mesophyll protoplasts treated with or without dexamethasone (DEX). GFP fluorescence was monitored using fluorescence microscopy. **E**) Measurements of GFP relative fluorescence intensity in protoplasts. Data are shown as means \pm SD. ******** $P \leq 0.0001$ by the Student's *t*-test. **F**) Examination of GFP accumulation before or after DEX treatment by immuno-blotting with anti-GFP antibody. For **E**), 80 to 100 cells were used for fluorescence intensity measurements. For **D and F**), experiments were independently conducted 3 times with similar results.

displayed equivalent actin cytoskeleton organizations at mature stages (Supplementary Fig. S9, B to D). *ttg2-6 brk1-1* trichomes exhibited similar morphological and actin-based phenotypes to those of *brk1-1* (Figs. 6, E to G, and 7, A to D; Supplementary Fig. S9, B to E). Meanwhile, we noticed that the genetic relationship between *BRK1* and *TTG2* was complex with respect to other trichome phenotypes. The branch numbers of *ttg2-6 brk1-1* trichomes were further decreased compared with the respective single mutants (Fig. 6B), while the trichome distribution and density were reminiscent of that of *ttg2-6* (Fig. 6, C and D). These results

suggest that *TTG2* may interact with *BRK1* to specifically regulate trichome branch initiation and polar growth in stalks and branches. In contrast, *TTG2* may integrate other pathways to control trichome cell differentiation and distribution.

To explore the potential interaction mechanisms between *TTG2* and *BRK1* during trichome development, we examined the expression level of *BRK1* in *ttg2* mutants. As illustrated in Fig. 8A, the transcripts of *BRK1* were slightly decreased in the absence of *TTG2*. To further confirm the effects of *TTG2* on *BRK1* expression, we generated *pBRK1:GUS* transgenic plants

and introduced the transgene into *ttg2-6* mutant by crossing. Consistent with the RT-qPCR data, the intensity of the GUS signals was much weaker in *ttg2-6* compared to those in the WT (Fig. 8B). Moreover, we observed that the GUS signals were mainly located in trichome cells in *pBRK1:GUS* plants (Fig. 8B), indicating a high expression of *BRK1* in trichome cells. We also assessed whether transiently increasing *TTG2* transcript level could stimulate *BRK1* expression through a protoplast effector/reporter assays. The effector vector *p35S:TTG2-GR* expressed a fusion protein with the glucocorticoid receptor (GR) and *TTG2* and the reporter vector was composed of 2 independent expression cassettes (Fig. 8C). When *p35S:TTG2-GR* was co-transfected with *pBRK1:GFP-pUBQ10:mCherry*, the GFP fluorescence signals were increased in DEX treated protoplasts compared with mock treatment (Fig. 8, D to F), demonstrating that elevated *TTG2* levels could promote *BRK1* promoter activity.

Due to the positive regulation of *TTG2* on *BRK1* expression, we hypothesized that overexpression of *BRK1* may rescue the trichome defects in *ttg2* mutant. To this end, we expressed fusion protein *BRK1-GFP* under the control of *BRK1* promoter in *ttg2-6* mutant to generate *ttg2-6 pBRK1:BRK1-GFP* transgenic plants. The *pBRK1:BRK1-GFP* construct could rescue the developmental impairments of *brk1-1* (Supplementary Fig. S10), suggesting that *BRK1-GFP* is functional in planta. However, the *ttg2-6 pBRK1:BRK1-GFP* plants produced unexpected trichome phenotypes. Although the trichome numbers were decreased, the overall trichome morphologies on the first pair of true leaves were similar to WT plants (Supplementary Fig. S11, A and B). However, aberrant trichomes similar to those in *ttg2-6* were observed on the subsequent leaves in *ttg2-6 pBRK1:BRK1-GFP* plants (Supplementary Fig. S11C).

TTG2 directly binds to the BRK1 promoter

The genetic and molecular interactions between *TTG2* and *BRK1* prompted us to investigate whether *BRK1* functions as a direct transcriptional target of *TTG2*. Since *TTG2* has been reported to bind to a conserved motif (T)(T)TGAC(C/T) termed W-boxes located in its targets promoters (Pesche et al. 2014; Fig. 9A), we therefore scanned the promoter region of *BRK1* for these consensus sequences. Three potential W-boxes were discovered located at –1078 to –1063 bp, –496 to –487 bp, and –150 to –141 bp (Fig. 9A), and were designated as W1, W2, and W3, respectively.

To test the direct binding of *TTG2* to these potential W-boxes in the *BRK1* promoter, we first adopted an in vitro fluorescence anisotropy (FA) assay which is a rapid, sensitive, and real-time assay to monitor the binding between proteins and DNA fragments (Xi and Deprez 2010). Within a given solution, the extent of depolarization depends on the rate of tumbling of the fluorescently labeled DNA molecule, which decreases with increasing size. Thus, when protein binds to a DNA molecule, accompanied by the increasing of the molecular size, the FA will increase compared to that of the free DNA molecule (Fig. 9B). According to these principles, 3 sequences covering each potential W-box in the *BRK1*

promoter were synthesized and modified with fluorescence group FAM, respectively. In addition, the His-*TTG2* recombinant proteins were expressed and purified. After measuring the value of the fluorescence anisotropy of solutions with the FAM modified DNA molecules alone and the solutions with both FAM modified DNA molecules and His-*TTG2* proteins, respectively, we found a remarkable alteration of FA in the combination that contained the W1 sequence and His-*TTG2* protein. Compared to the other 2 sequences, His-*TTG2* could bind to W1 sequence in a low concentration (Fig. 9C), with a lower K_d of 9.26 (Fig. 9D). Meanwhile, we performed electrophoretic mobility gel shift assay (EMSA) experiment to further confirm the binding of *TTG2* to W1 region as well. As shown in Fig. 9E, the presence of His-*TTG2* protein retarded the shift of W1 probe in the gel. Consistently, the retardation was remarkably weakened when no-labeled competitive probes were added. Mutation of the W1 sequence could also apparently impaired the binding.

To test if *TTG2* could bind to the *BRK1* promoter in planta, we carried out chromatin immunoprecipitation followed by quantitative PCR (ChIP-qPCR) analyses. The above ground tissues of 2-wk-old *pTTG2:TTG2-GFP* plants were harvested, and ChIP was carried out with GFP-Trap agarose beads. The *pTTG2:TTG2-GFP* construct is functional since expression of *pTTG2:TTG2-GFP* could restore the trichome developmental defects either in *ttg2-6* or in *ttg2-7* background (Supplementary Fig. S12). Consistent with the results from in vitro experiments, we found that the W1 fragments were significantly enriched in the immunoprecipitated DNA compared with other 2 fragments (Fig. 9F), indicating a direct binding of *TTG2* to the W1 fragment in *BRK1* promoter.

Taken together, we propose a model in which *TTG2* is required at all stages during trichome development. It influences the early stage of trichome specification through its control of *TRY*. During the trichome cell morphogenesis, *TTG2* regulates proper branching by dictating cell cycle processes and cMTs configurations. During the later stages when the established pattern is elaborated, *TTG2* maintains the extension growth of the trichome stalks and branches via direct association with the actin cytoskeleton (Fig. 10).

Discussion

The unique trichome morphologies in *ttg2-6*

In previous reports, functional loss of *TTG2* was shown to induce trichomes with reduced branch numbers (Johnson et al. 2002). However, *ttg2-6* displays varied branched trichomes, ranging from 1 to 7-branched, and even 9-branched trichomes (Fig. 1, E to G and H). Such a trichome phenotype is really interesting, because to date, almost all of the trichome branching defective mutants reported display consistently branching phenotypes, with either less-branched or over-branched trichome (Tominaga-wada et al. 2011; Li et al. 2019; Han et al. 2022). Moreover, the trichome phenotypes of *ttg2-6* also seem inconsistent with other *ttg2*

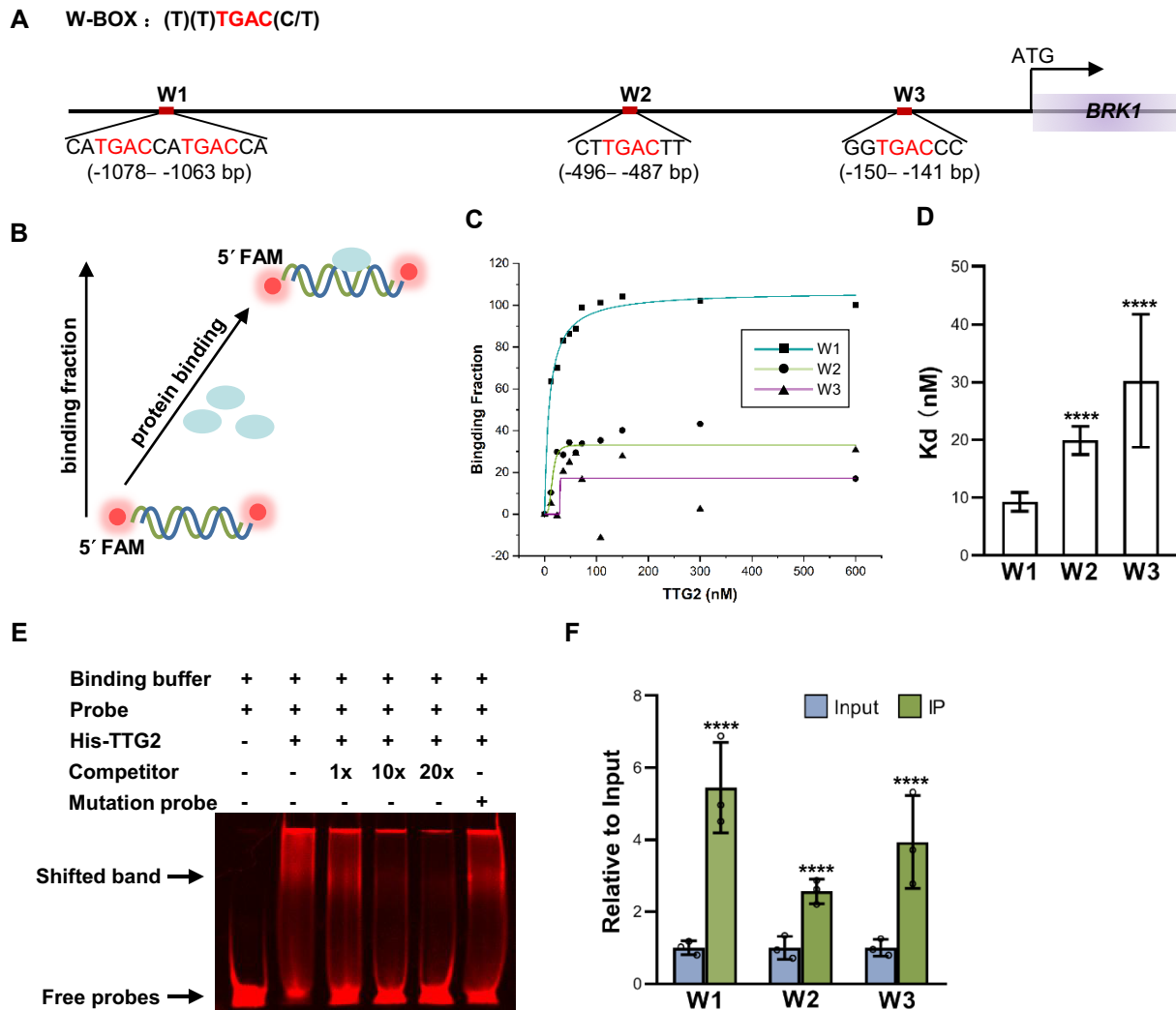


Figure 9. Binding of TTG2 to the *BRK1* promoter. **A**) The consensus sequence of the W-box, and potential W-box locations in the *BRK1* promoter. **B**) Schematic illustration of the FA experiment. The fluorescein FAM labeled oligonucleotide alone gives a low steady-state anisotropy value. Upon proteins (ovals) binding to the DNA molecule, the fluorescence anisotropy increases. The binding fraction was calculated by subtracting the steady-state fluorescence anisotropy from that when protein was added. Therefore, the direct binding of the protein to the target DNA molecular leads to an increase of binding fraction. **C and D**) Measurements of binding fraction **C**) and the K_d **D**) values in the FA experiment. The steady-state fluorescence anisotropy was determined before and after the addition of different concentrations of His-TTG2, respectively. The binding plots were simulated by using the Origin software. The K_d value was obtained through a Hill fit of the fluorescence anisotropy data. **E**) EMSA assay of the directly binding of TTG2 to W1 fragments on *BRK1* promoter. The 1-, 10-, and 20-fold excess nonlabeled probes and mutation probes were used as the competitor. **F**) Chromatin immunoprecipitation-qPCR (ChIP-qPCR) analyses of the binding activities of TTG2 to W1 to W3 fragments on *BRK1* promoter. The enrichment values are displayed as the ratio between the input and immunoprecipitated (IP) DNAs. Data were means \pm SD for 3 biological replicates. **** $P \leq 0.0001$ by the Student's *t*-test.

alleles both whatever in *Ler* or in *Col* background in other aspects. For example, although it has been reported that some trichomes in *ttg2-1* and *ttg2-3* show a range of distorted growth patterns (Johnson et al. 2002; Ishida et al. 2007; Fig. 3), it is not as remarkable as that in *ttg2-6* (Fig. 1, B, E, and G). One of the possible explanations is that *ttg2-6* may represent a weak mutant allele of *TTG2*. First, the overall trichome branch numbers are reduced in *ttg2-6* (Fig. 1, H and I), which is consistent with other *ttg2* alleles (Johnson et al. 2002; Ishida et al. 2007; Fig. 3).

Second, like that in *ttg2-3*, the expression pattern of *CPC*, *GL2*, and *TRY* was also altered in *ttg2-6* mutant (Supplementary Fig. S13). Third, in contrast to other *ttg2* mutants, the mutation occurs at the very C-terminal in *ttg2-6* (Fig. 2, A and B), which may allow partial functions of *TTG2* to be preserved. Meanwhile, given that mutation site in *ttg2-6* happens in 1 of the 2 conserved Cys residues in the second putative zinc finger motif (Johnson et al. 2002; Fig. 2A), the Cys residue therefore might be critical for *TTG2* in regulating trichome branching.

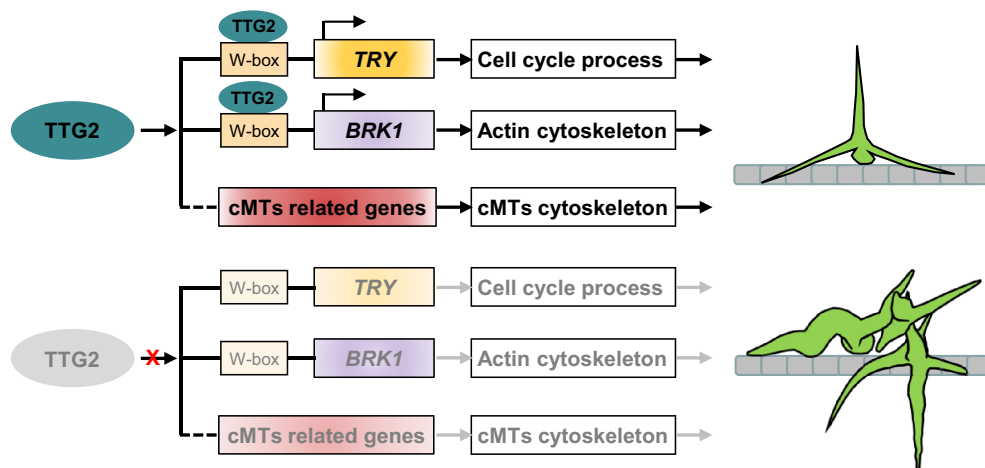


Figure 10. The proposed working model for *TTG2* in controlling trichome development. *TTG2* is required for trichome development at all stages. During early stage, it controls trichome specification through controlling the expression of single repeat MYB transcription factor *TRY*. At the stage of trichome cell morphogenesis, *TTG2* regulates proper branch numbers by dictating cell cycle processes and cMTs configurations. During the stages of trichome branch growth, *TTG2* maintains the extension directions of the trichome branches via direct association with the actin cytoskeleton. cMTs, cortical microtubules. Arrows represent positive regulation of the target genes while the cross indicates the inhibition of the expression of the targets. The solid lines represent the direct molecular interactions while the dotted lines indicate the indirect or unidentified molecular pathways.

Collectively, the isolation of the *ttg2-6* mutant provides a distinct genetic material to further unravel the molecular function of *TTG2* in modulating trichome development.

TTG2 integrates microtubule cytoskeletal and cell cycle signals to control trichome branching

Accumulated information have demonstrated cell cycle control and microtubule organization are 2 essential pathways required for trichome branch initiation (Mathur and Chua 2000; Schnittger and Hülskamp 2002; Szymanski 2005; Li et al. 2019). Generally, the nuclear DNA content of mature trichomes will reach to 32C (C equals haploid DNA content per nucleus), accompanied by the formation of 3 or 4 branches (Schnittger and Hülskamp 2002). Mutations in genes that increase or decrease the endoreduplication levels elevate or reduce the nuclei size and the number of branches respectively (Tominaga-Wada et al. 2011; Han et al. 2022). Meanwhile, during trichome morphogenesis, the arrangement of cMTs changes dramatically at branching points (Mathur and Chua 2000; Sambade et al. 2014; Li et al. 2019). Mutation in genes involved in the cMTs assemble or dynamics often leads to aberrant trichome branching (Tominaga-Wada et al. 2011; Li et al. 2019). Given the production of remarkable over-branched trichomes in *ttg2-6* (Fig. 1, B and E to I), we examined the trichome nuclear size in *ttg2-6* (see Supplemental Methods) and revealed an apparent increased nuclei size and nuclear DNA content (Supplementary Fig. S14, A to C). We also verified global DNA ploidy levels in *ttg2-6* plants with flow cytometry (see Supplemental Methods). Compared to that in WT, a marked shift of cells to higher ploidy levels was observed in *ttg2-6* (Supplementary Fig. S14D). In consistent, the *ttg2-6* plants

displayed enlarged cotyledons (Supplementary Fig. S14, E and G) and cotyledon pavement cell sizes compared with those of the WT (Supplementary Fig. S14, F and H). These findings suggest that *TTG2* may be involved in the endoreduplication regulation during trichome morphogenesis and also provide genetic evidences for the previous report that *TTG2* directly activates the expression of *TRY* that regulates trichome morphologies in a cell cycle-dependent manner (Szymanski and Marks 1998; Pesch et al. 2014). Hence, *TRY* may mediate the regulation of *TTG2* on cell cycle control.

Meanwhile, the cMTs arrangements are obviously disrupted (Supplementary Fig. S4) in *ttg2-6*, establishing a connection of *TTG2* on the microtubule cytoskeleton regulation. To elaborate the underlying mechanisms of the regulations of *TTG2* on cMTs, we crossed *ttg2-6* with those trichome branching mutants associated with cMTs assembly or dynamics reported before to implement genetic interaction analyses. Additive effects were observed by examining the trichome phenotypes of different combinations (Supplementary Figs. S5 and S6), suggesting that *TTG2* may act in cooperating with these genetic factors to regulate microtubule cytoskeleton during trichome development. Therefore, other strategies such as RNA-seq or ChIP-seq could be employed to screen the potential *TTG2* targets associated with microtubule cytoskeletal pathway.

TTG2 regulates trichome branching expansion through directly interacting with actin cytoskeletal component

In addition to show trichome branching defects, a proportion of trichomes in *ttg2-6* display striking distorted phenotypes (Fig. 1, E and G), resembling to that of the *SCAR/WAVE* and

ARP2/3 mutants (Hülkamp et al. 1994; Schwab et al. 2003; Szymanski 2005; Li et al. 2019). This phenotypic association implies the function of *TTG2* on actin cytoskeletal organization. As respected, we observed that the F-actin organization is dramatically disrupted in *ttg2-6* trichomes (Fig. 5). Genetic analyses indicate that *brk1* is epistasis to *ttg2-6* with regard to branching expansion (Figs. 6 and 7). *BRK1* encodes a member of SCAR/WAVE complex and participates in ARP2/3 activation (Gallagher and Smith 2000; Frank and Smith 2002; Djakovic et al. 2006; Le et al. 2006). Mutation of *BRK1* results in distorted trichome morphology and aberrant F-actin cytoskeleton organization (Gallagher and Smith 2000; Frank and Smith 2002; Djakovic et al. 2006). Further, we found that the expression of *BRK1* is positively regulated by *TTG2* (Fig. 8), indicating that *BRK1* may serve as a potential target of *TTG2*. Additional biochemical and molecular experiments showed *TTG2* could directly bind to a W-box in the *BRK1* promoter (Fig. 9). These findings suggest that the effect of *TTG2* on actin cytoskeleton organization may be achieved through directly modulating the expression of *BRK1*. In addition, we found that the transcript accumulation of *BRK1* is apparently inhibited in *gl1*, *ttg1*, and *gl3* mutants, and the trichome phenotypes of *gl1 brk1-1*, *ttg1 brk1-1*, and *gl3 brk1-1* double mutants resemble the *brk1-1* single mutant respectively (Supplementary Fig. S15). These preliminary results suggest that *BRK1* may act downstream of the MYB-bHLH-WD-40 transcription activation complex, further supporting our data that *TTG2* acts upstream of *BRK1* to modulate trichome morphogenesis.

Conclusions

Taking advantages of the isolation of *ttg2-6* mutant, we uncover previous unknown functions of *TTG2* and suggest that *TTG2* is required at all stages of during trichome development. In addition, our studies directly link *TTG2* and actin cytoskeletal component, providing important insight into cellular signaling events downstream of the transcriptional factors associated with trichome development in Arabidopsis.

Materials and methods

Plant materials and growth conditions

Plant materials used in this study are all in the Arabidopsis (*A. thaliana*) Columbia-0 (*Col-0*) background except for the map-based cloning. The wide type (WT) refers to *Col-0* plants. T-DNA insertion lines for *TTG2* (*Salk_148838*, *ttg2-3*; *Salk_206852*, *ttg2-7*) (Ishida et al. 2007), *BRK1* (*CS86554*, *brk1-1*; *CS93199*, *brk1-2*) (Djakovic et al. 2006), *ZWI* (*Salk_017886*, *zwi-101*) (Chen et al. 2016), *AN* (*Salk_026489*) (Gachomo et al. 2013), *KTN1* (*Sail_343_D12*) (Chen et al. 2014), *CRK* (*Salk_123936*) (Bellinvia et al. 2022), *WRM* (*Salk_003448*) (Le et al. 2003), *DIS2* (*Salk_201281*), *IBT* (*Salk_039449*) (Uhrig et al. 2007), *GRL* (*Salk_135634*) (El-Assal et al. 2004), *GL1* (*SALK_133117*), *TTG1* (*CS67772*, *ttg1-13*), *gl3-1* (Koornneef et al. 1982), and a marker line for microtubule array *GFP-TUB6* (*CS6550*) (Liang et al. 2019)

were obtained from the Arabidopsis Biological Resource Center (ABRC). The *ttg1-13* and *gl3-1* lines were crossed 3 times to *Col-0* respectively before used for construction double mutants. Double mutants were constructed by crossing. The T-DNA insertion sites and homozygous plants were confirmed by genomic PCR and DNA sequencing. The marker line for actin filaments *ABD2-GFP* was kindly provided by Prof. Zhaosheng Kong (Chinese Academy of Sciences). Primers used for genotyping were listed in Supplementary Table S1.

For plant culture, seeds were stratified at 4 °C for 2 d and then sowed on commercial soil mix (Pindstrup, Denmark) for germinating and growth in growth room at 22 ± 1 °C under continuous illumination (~100 μmol m⁻² s⁻¹). For protoplast preparation, seeds were sowed and grown on Jiffy-7-Peat Pellets (Jiffy Group, Netherlands) in a growth chamber (Convicon A1000, Canada) with day/night cycle (12 h/12 h) at 22 ± 1 °C, and fully expanded rosette leaves of 30-d-old plants were used.

Trichome phenotype characterization

Trichome phenotypes were examined as described by Liang et al. (2019). For each genotype, at least 15 individuals were used for quantitative analysis, and all experiments were repeated for 3 times. Quantitative investigation of trichome morphologies at appropriately developmental stages were performed according to Szymanski et al. (1999, 2001). The width and length of various staged trichomes on the fourth true leaves of 10-d-old Murashige and Skoog (MS) medium grown seedlings were measured. For each genotype, at least 15 to 20 independent trichomes were used for statistical analyses.

For all quantitative analyses, Student's *t*-test was used to assess the statistical significance.

Mutant screening and map-based cloning

The *abt4-1* (*ttg2-6*) mutant was isolated from an ethyl methanesulfonate (EMS)-mutagenesis mutant population in *gl2-3* mutant background (*Salk_039825*, Wang et al. 2010) we established before. The *abt4-1 gl2-3* double mutants were initially isolated with transparent and distorted trichome. The *abt4-1* single mutant was obtained by backcrossing the *abt4-1 gl2-3* mutant with *Col-0* plants, and 2 additional rounds of backcross were carried out before phenotypic characterization.

The mutation site in *abt4-1* was determined via map-based cloning according to Lukowitz et al. (2000). Sequence information of the molecular markers used were listed in the Supplementary Table S1.

Generation of transgenic plants

The *pTTG2:TTG2* plasmid was constructed by cloning genomic fragment comprising the 1,086 bp endogenous promoter and the full-length coding region of *TTG2* into pCambia 1300 vector with *XbaI* and *KpnI* to conduct complementation experiments. To evaluate the effects of *BRK1*

on trichome development in *ttg2* mutant background, the *pBRK1:BRK1-GFP* plasmid was generated by fusing the genomic fragment of *BRK1* including the 1,515 bp promoter sequences to *GFP* gene and cloning of the fused sequences into pCAMBIA 1300 vector with *Xba*I and *Bam*HI. *pTTG2:TTG2-GFP* construct was generated by using the similar procedures with *Xba*I to perform the ChIP experiment. *pBRK1:GUS*, *pCPC:GUS*, *pGL2:GUS*, and *pTRY:GUS* plasmids were obtained by introducing the promoter sequence of *BRK1*, *CPC*, *GL2*, and *TRY* into the upstream of *GUS* gene in pCB308 vector with *Xba*I, *Bam*HI, *Bam*HI, and *Xba*I and *Bam*HI, respectively. All the primers used were listed in [Supplementary Table S1](#).

The confirmed constructs were transformed into the indicated genetic background via *Agrobacterium* (*Agrobacterium tumefaciens* strain EHA105) mediated floral-dip method ([Clough and Bent 1998](#)). Transgenic plants were obtained through antibiotic-resistant, genomic PCR, and trichome phenotype examination, respectively. The T3 plants were used for phenotype characterization and other experiments. At least 20 independent transgenic lines were obtained for each transformation, and 2 representatives were used for detailed analyses.

RNA isolation and RT-qPCR

Total RNAs were extracted from the fifth to seventh rosette leaves of 2-wk-old soil grown plants with TRIzol reagent (15596026, Thermo Fisher Scientific, United States of America). cDNAs were obtained with oligo (dT)₁₅ primer by using the Maxima H Minus cDNA Synthesis Master Mix (M1662, Thermo Fisher Scientific). qPCR was carried out with the Fast Start Essential DNA Green Master kit (06402712001, Roche, Switzerland) and Bio-Rad CFX96 real-time PCR system. Relative expression levels of the target genes were calculated with $2^{-\Delta\Delta C_t}$. Expressions of *ACTIN2* (*ACT2*) were used as the internal controls. Primers for qPCR were listed in [Supplementary Table S1](#).

Cortical microtubules (cMTs) and actin filaments (F-actin) imaging and quantification

To achieve living cell cortical microtubules (cMTs) and actin filaments (F-actin) observation, marker lines *CS6550* (*GFP-TUB6*) and *ABD2-GFP* were crossed into different mutant background and the double mutants were selected by GFP fluorescence examination. Trichomes in appropriate developmental stages on the fourth true leaves of MS medium grown seedlings were examined for green fluorescence under a spinning disk confocal system built on a DMI8 inverted microscope (Leica, Germany) equipped with a CSU-W1 confocal scanner unit (Yokogawa, Japan) and an iXon Ultra 888 EMCCD camera (Andor, Northern Ireland). cMTs and F-actin were observed with a HCPLAPO 63× or 100× N.A.1.30 glycerol objective (Leica), and images were taken through Z-stacking with a 0.5 μm z-step. GFP was excited at

488 nm, and the emission wavelength was 507 nm. The excitation intensity was 25%, and EM gain was 106.

Images were processed and analyzed using Fiji ImageJ software. F-actin quantification was performed according to [Le et al. \(2003\)](#) and [El-Assal et al. \(2004a\)](#). The relative amounts of core cytoplasmic and cortical actin filaments were measured at the midpoint ± 1.3 μm between the stalk apex and the upper edge of the nucleus at Stage 2 and the midpoint ± 1.3 μm of Stage 3/4 and 4/5 branches. The cortical domain of the branch was defined as a 2.5 μm wide band that included the plasma membrane at the outer edge. Total actin filaments intensity is defined as cortical plus core cytoplasmic actin filaments signals. Trichomes below than 40 μm in height in the WT, *brk1-1*, and *ttg2-6 brk1-1* background were used in the assay. Considering the larger trichome size in *ttg2-6*, cells with a height no more than 75 μm were used in the measurements, which is equivalent to about 40 μm in height in the WT. The F-actin angles and anisotropy were evaluated according to [Boudaoud et al. \(2014\)](#) and [Chang et al. \(2019\)](#), and the following convention was used: the anisotropy score 0 for no order (purely isotropic arrays) and 1 for perfectly ordered (purely anisotropic arrays). The value of F-actin angles of that parallel to the trichome branch or stalk extension directions was defined as 0°, while the value of those were perpendicular to the cell's longitudinal axis was defined as 90°.

Protoplast effector/reporter assays

The experimental procedures were conducted according to [Iwata et al. \(2011\)](#). The reporter plasmid *pBRK1:GFP-pUBQ10:mCherry* and effector plasmid *p35S:TTG2-GR* were constructed with *Bam*HI and transient expression vector pTF486, respectively. Primers used were listed in [Supplementary Table S1](#). The mesophyll protoplast from WT leaves was prepared, and the reporter and effector plasmids (20 μg each) were co-transformed into 200 μL mesophyll protoplasts according to [Yoo et al. \(2007\)](#). After transfection, protoplasts were treated with 5 μM dexamethasone (DEX) or equal volume of ethanol and incubated in W5 buffer (154 mM NaCl, 125 mM CaCl₂, 5 mM KCl, 2 mM MES) for 12 h. The fluorescence signals were examined under a fluorescence microscope (DMI8, Leica, Germany), and mCherry fluorescence was used as the transfection control. The excitation and emission wavelength were 450 to 490 nm and 500 to 550 nm for GFP and 590 to 650 nm and 662 to 738 nm for mCherry, respectively. For each transfection, more than 100 protoplasts which showed mCherry signals were used to measure GFP fluorescence signal intensity with ImageJ software. The experiments were repeated for 3 times with similar results.

FA experiment

The FA experiment was employed according to [Xi and Deprez \(2010\)](#). First, the recombinant protein His-TTG2 was obtained by inducing expression of *pET28a-His-TTG2* constructed with *Bam*HI in *Escherichia coli* strain Rosetta (DE3)

and purifying soluble proteins through affinity chromatography with Ni²⁺-nitrilotriacetate acid columns followed by fast protein liquid chromatography with size exclusion chromatography columns according to manufacturer's specifications. Primers used for plasmid construction were listed in [Supplementary Table S1](#). Second, the fragments which carry the potential W-box in the *BRK1* promoter were synthesized and modified with fluorescence group FAM at the 3' and 5' ends, respectively. Third, the FAM modified DNA fragments were annealed, and the steady-state fluorescence anisotropy of the double strand DNA was evaluated with a commercial fluorescence polarization system (Beacon 2000 Fluorescence Polarization, PanVera Corporation, United States of America). Lastly, the His-TTG2 protein was added at the indicated concentrations, and the fluorescence anisotropy value of the solution was measured. The binding fraction is calculated by subtracting the steady-state fluorescence anisotropy from that when His-TTG2 protein was added. The dissociation constant (K_d) were calculated according to $\Delta r = \Delta r_{\max} \times \frac{P}{K_d + P}$, where P corresponds to protein concentration, Δr and Δr_{\max} represent the value of fluorescence anisotropy and maximal fluorescence anisotropy difference, respectively.

EMSA

The probes covering the W1 region in *BRK1* promoter (50 bp in length) were commercially synthesized and labeled with Cy5 by Sangon Biotech (Shanghai, China). EMSA was performed according to [Wang et al. \(2022\)](#). Reaction system was prepared by mixing 4 μ L 5 \times binding buffer (1 M Tris pH 7.5, 5 M NaCl, 1 M KCl, 1 M MgCl₂, 0.5 M EDTA, 1 M DTT, 10 mg/mL BSA), 300 ng purified His-TTG2, and 500 nM labeled DNA probes in a 20 μ L reaction volume and incubated on ice at dark for 30 min. The reaction products were electrophoresed using 6% (w/v) native polyacrylamide gels and the fluorescence signal in the gel was visualized using an infrared fluorescence imaging system (FluorChem R, Protein Simple, United States of America). The excitation and emission wavelength were 680 and 720 nm, respectively. Nonlabeled and mutated probes were used as competitors. The sequence of the probes was listed in [Supplementary Table S1](#).

Chromatin immunoprecipitation (ChIP) experiment

The experiment was performed according to [Wang et al. \(2022\)](#). 3 to 4 g of leaf samples from 2-wk-old soil grown *pTTG2:TTG2-GFP* plants was harvested and fixed with cross-linking buffer (10 mM Tris-HCl pH 8.0, 0.4 M sucrose, 10 mM MgCl₂, 5 mM β -ME, 1 mM PMSF, and 1% formaldehyde (v/v)) for 10 min under vacuum. The treated tissues were ground in liquid nitrogen, and the nuclei were extracted and collected with extraction buffer (0.4 M sucrose, 10 mM Tris-HCl pH 8.0, 10 mM MgCl₂, 5 mM mercaptoethanol, 0.1 mM phenylmethanesulfonyl fluoride, 1 \times protease inhibitor) and nuclear lysis buffer (50 mM Tris-HCl pH 8.0, 10 mM EDTA, 1% (w/v) SDS, 1 mM PMSF, 1 \times protease inhibitor cocktail). The lysate was sonicated with Bioruptor Pico

(Diagenode, United States of America), and the resulting solution was incubated with GFP-Trap agarose beads (gta-20, Chromo Tek, Germany) at 4 °C overnight with gentle shaking to immunoprecipitate chromatin complexes. The immunoprecipitated DNAs were obtained from the complexes through reverse crosslinking, proteinase K (EO0491, Thermo Fisher Scientific) digestion, and purification with QIAquick PCR Purification Kit (28104, Qiagen, Germany). DNA levels in input and immunoprecipitated solutions were determined by qPCR, and fold enrichments were calculated as the ration between the input and immunoprecipitated DNAs. A PP2A fragment was used as the nonbinding control in qPCRs. Primers used were listed in [Supplementary Table S1](#). The experiments were repeated for 3 times with similar trends.

Accession numbers

Sequence data from this article can be found in the TAIR/GenBank database with the accession numbers shown in [Supplementary Table S2](#).

Acknowledgments

We thank Prof. Hou (Northwest A&F University) for the technical support for FA experiment.

Author contributions

L.A., L.L., and Y.W. conceived the project and arranged the experiments. L.L., Y.W., W.C., L.Yang, C.Z., L.Yuan, and D.W. performed the experiments; L.A., L.L., Y.W., and W.W. analyzed the data; L.L., Y.W., and L.A. wrote the manuscript; H.Z., F.Y., and J.S. revised the manuscript.

Supplementary data

The following materials are available in the online version of this article.

[Supplementary Table S1](#). Primer pairs used in this work.

[Supplementary Table S2](#). Accession numbers for the genes cited in this work.

[Supplementary Methods](#).

[Supplementary Figure S1](#). The overall plant morphology of *abt4-1*.

[Supplementary Figure S2](#). Map-based cloning of the *ABT4* locus.

[Supplementary Figure S3](#). Quantitative examination of stalk and branch phenotypes in *ttg2-6* mature trichomes.

[Supplementary Figure S4](#). Arrangements of cMTs in *ttg2-6* trichomes at different developmental stages.

[Supplementary Figure S5](#). Trichome phenotypes of the *ttg2-6 zwi-101* plants.

[Supplementary Figure S6](#). Trichome phenotypes of the *ttg2-6* and *ttg2-6 ktn1-1* plants.

[Supplementary Figure S7](#). Trichome phenotypes of the double mutant combined with *ttg2-6* and different *ARP2/3* mutants.

Supplementary Figure S8. Trichome phenotypes of the double mutant combined with *ttg2-6* and different SCAR/WAVE mutants.

Supplementary Figure S9. The overall plant morphology and F-actin arrangements in mature trichomes in *ttg2-6 brk1-1*.

Supplementary Figure S10. Complementation of the *brk1-1* mutant with the *pBRK1:BRK1-GFP* construct.

Supplementary Figure S11. Trichome phenotypes of *ttg2-6 pBRK1:BRK1-GFP* plants.

Supplementary Figure S12. Complementation of the *ttg2* mutants with the *pTTG2:TTG2-GFP* construct.

Supplementary Figure S13. Expression patterns of *CPC*, *GL2*, and *TRY* in *ttg2-6*.

Supplementary Figure S14. Characterization of DNA ploidy in *ttg2-6*.

Supplementary Figure S15. Genetic analyses of the MYB-bHLH-WD-40 transcription complex and *BRK1* in trichome morphogenesis.

Funding

This work is supported by the National Natural Science Foundation of China (31470290, 32070198), the Chinese Universities Scientific Fund (2452020180), and the National Science Foundation (1923589 and IOS-2127485).

Conflict of interest statement. None declared.

Data availability

All data are incorporated into the article and its online supplementary material.

References

- Arteaga N, Méndez-Vigo B, Fuster-Pons A, Savic M, Murillo-Sánchez A, Picó FX, Alonso-Blanco C.** Differential environmental and genomic architectures shape the natural diversity for trichome patterning and morphology in different *Arabidopsis* organs. *Plant Cell Environ.* 2022;**45**(10):3018–3035. <https://doi.org/10.1111/pce.14308>
- Basu D, El-Din El-Assal S, Le J, Mallery EL, Szymanski DB.** Interchangeable functions of *Arabidopsis* PIROGI and the human WAVE complex subunit SRA1 during leaf epidermal development. *Development.* 2004;**131**(17):4345–4355. <https://doi.org/10.1242/dev.01307>
- Basu D, Le J, El-Din El-Assal S, Huang S, Zhang C, Mallery EL, Koliantz G, Staiger CJ, Szymanski DB.** DISTORTED3/SCAR2 is a putative *Arabidopsis* WAVE complex subunit that activates the Arap2/3 complex and is required for epidermal morphogenesis. *Plant Cell.* 2005;**17**(2):502–524. <https://doi.org/10.1105/tpc.104.027987>
- Basu D, Le J, Zakharova T, Mallery EL, Szymanski DB.** A SPIKE1 signaling complex controls actin-dependent cell morphogenesis through the heteromeric WAVE and ARP2/3 complexes. *Proc Natl Acad Sci USA.* 2008;**105**(10):4044–4049. <https://doi.org/10.1073/pnas.0710294105>
- Bellinvia E, García-González J, Cifrová P, Martinek J, Sikorová L, Havelková L, Schwarzerová K.** CRISPR-Cas9 *Arabidopsis* mutants of genes for ARPC1 and ARPC3 subunits of ARP2/3 complex reveal differential roles of complex subunits. *Sci Rep.* 2022;**12**(1):18205. <https://doi.org/10.1038/s41598-022-22982-8>
- Boudaoud A, Burian A, Borowska-Wykręt D, Uyttewaal M, Wrzalik R, Kwiatkowska D, Hamant O.** FibrilTool, an ImageJ plug-in to quantify fibrillar structures in raw microscopy images. *Nat Protoc.* 2014;**9**(2):457–463. <https://doi.org/10.1038/nprot.2014.024>
- Chang J, Xu Z, Li M, Yang M, Qin H, Yang J, Wu S.** Spatiotemporal cytoskeleton organizations determine morphogenesis of multicellular trichomes in tomato. *PLoS Genet.* 2019;**15**(10):e1008438. <https://doi.org/10.1371/journal.pgen.1008438>
- Chen L, Peng Y, Tian J, Wang X, Kong Z, Mao TL, Yuan M, Li Y.** TCS1, a microtubule-binding protein, interacts with KCBP/ZWICHEL to regulate trichome cell shape in *Arabidopsis thaliana*. *PLoS Genet.* 2016;**12**(10):e1006266. <https://doi.org/10.1371/journal.pgen.1006266>
- Chen X, Grandont L, Li H, Hauschild R, Paque S, Abuzeineh A, Rakusová H, Benkova E, Perrot-Rechenmann C, Friml J.** Inhibition of cell expansion by rapid ABP1-mediated auxin effect on microtubules. *Nature.* 2014;**516**(7529):90–93. <https://doi.org/10.1038/nature13889>
- Chin S, Kwon T, Khan BR, Sparks JA, Mallery EL, Szymanski DB, Blancaflor EB.** Spatial and temporal localization of SPIRRIG and WAVE/SCAR reveal roles for these proteins in actin-dependent root hair development. *Plant Cell.* 2021;**33**(7):2131–2148. <https://doi.org/10.1093/plcell/koab115>
- Clough SJ, Bent AF.** Floral dip: a simplified method for *Agrobacterium* mediated transformation of *Arabidopsis thaliana*. *Plant J.* 1998;**16**(6):735–743. <https://doi.org/10.1046/j.1365-313x.1998.00343.x>
- Deeks MJ, Kaloriti D, Davies B, Malhó R, Hussey PJ.** *Arabidopsis* NAP1 is essential for Arp2/3-dependent trichome morphogenesis. *Curr Biol.* 2004;**14**(15):1410–1414. <https://doi.org/10.1016/j.cub.2004.06.065>
- Djakovic S, Dyachok J, Burke M, Frank MJ, Smith LG.** BRICK1/HSPC300 functions with SCAR and the ARP2/3 complex to regulate epidermal cell shape in *Arabidopsis*. *Development.* 2006;**133**(6):1091–1100. <https://doi.org/10.1242/dev.02280>
- Dyachok J, Shao M-R, Vaughn K, Bowling A, Facette M, Djakovic S, Clark L, Smith LG.** Plasma membrane-associated SCAR complex subunits promote cortical F-actin accumulation and normal growth characteristics in *Arabidopsis* roots. *Mol Plant.* 2008;**1**(6):990–1006. <https://doi.org/10.1093/mp/ssn059>
- Dyachok J, Zhu L, Liao F, He J, Huq E, Blancaflor EB.** SCAR mediates light-induced root elongation in *Arabidopsis* through photoreceptors and proteasomes. *Plant Cell.* 2011;**23**(10):3610–3626. <https://doi.org/10.1105/tpc.111.088823>
- El-Assal SED, Le J, Basu D, Mallery EL, Szymanski DB.** *Arabidopsis* GNARLED encodes a NAP125 homolog that positively regulates ARP2/3. *Curr Biol.* 2004a;**14**(15):1405–1409. <https://doi.org/10.1016/j.cub.2004.06.062>
- El-Din El-Assal S, Le J, Basu D, Mallery EL, Szymanski DB.** DISOTRED2 encodes an ARPC2 subunit of the putative *Arabidopsis* ARP2/3 complex. *Plant J.* 2004b;**38**(3):526–538. <https://doi.org/10.1111/j.1365-313X.2004.02065.x>
- Folkers U, Berger J, Hülskamp M.** Cell morphogenesis of trichomes in *Arabidopsis*: differential control of primary and secondary branching by branch initiation regulators and cell growth. *Development.* 1997;**124**(19):3779–3788. <https://doi.org/10.1242/dev.124.19.3779>
- Frank MJ, Smith LG.** A small, novel protein highly conserved in plants and animals promotes the polarized growth and division of maize leaf epidermal cells. *Curr Biol.* 2002;**12**(10):849–853. [https://doi.org/10.1016/S0960-9822\(02\)00819-9](https://doi.org/10.1016/S0960-9822(02)00819-9)
- Gachomo EW, Jimenez-Lopez JC, Smith SR, Cooksey AB, Oghoghomeh OM, Johnson N, Baba-Moussa L, Kotchoni SO.** The cell morphogenesis *ANGUSTIFOLIA* (*AN*) gene, a plant homolog of CtBP/BARS, is involved in abiotic and biotic stress response in higher plants. *BMC Plant Biol.* 2013;**13**(1):79. <https://doi.org/10.1186/1471-2229-13-79>
- Gallagher K, Smith LG.** Roles for polarity and nuclear determinants in specifying daughter cell fates after an asymmetric division in the maize leaf. *Curr Biol.* 2000;**10**(19):1229–1232. [https://doi.org/10.1016/S0960-9822\(00\)00730-2](https://doi.org/10.1016/S0960-9822(00)00730-2)

- Han G, Li Y, Yang Z, Wang C, Zhang Y, Wang B.** Molecular mechanisms of plant trichome development. *Front Plant Sci.* 2022;**13**:910228. <https://doi.org/10.3389/fpls.2022.910228>
- Hülkamp M, Misera S, Jürgens G.** Genetic dissection of trichome cell development in *Arabidopsis*. *Cell.* 1994;**76**(3):555–566. [https://doi.org/10.1016/0092-8674\(94\)90118-X](https://doi.org/10.1016/0092-8674(94)90118-X)
- Hülkamp M.** Plant trichomes: a model for cell differentiation. *Nat Rev Mol Cell Biol.* 2004;**5**(6):471–480. <https://doi.org/10.1038/nrm1404>
- Ishida T, Hatton S, Sano R, Inoue K, Shirano Y, Hayashi H, Shibata D, Sato S, Kato T, Tabata S, et al.** *Arabidopsis* TRANSPARENT TESTA GLABRA2 is directly regulated by R2R3 MYB transcription factors and is involved in regulation of GLABRA2 transcription in epidermal differentiation. *Plant Cell.* 2007;**19**(8):2531–2543. <https://doi.org/10.1105/tpc.107.052274>
- Iwata Y, Lee MH, Koizumi N.** Analysis of a transcription factor using transient assay in *Arabidopsis* protoplasts. *Methods Mol Biol.* 2011;**754**:107–117. https://doi.org/10.1007/978-1-61779-154-3_6
- Johnson CS, Kolevski B, Smyth DR.** TRANSPARENT TESTA GLABRA2, a trichome and seed coat development gene of *Arabidopsis*, encodes a WRKY transcription factor. *Plant Cell.* 2002;**14**(6):1359–1375. <https://doi.org/10.1105/tpc.001404>
- Jörgens C, Grünwald N, Hülkamp M, Uhrig JF.** A role of ABIL3 in plant cell morphogenesis. *Plant J.* 2010;**62**(6):925–935. <https://doi.org/10.1111/j.1365-3113X.2010.04210.x>
- Koornneef M, Dellaert LW, van der Veen JH.** EMS- and radiation-induced mutation frequencies at individual loci in *Arabidopsis thaliana*. *Mutat Res.* 1982;**93**(1):109–123. [https://doi.org/10.1016/0027-5107\(82\)90129-4](https://doi.org/10.1016/0027-5107(82)90129-4)
- Le J, El-Assal SED, Basu D, Saad ME, Szymanski DB.** Requirements for *Arabidopsis* ATARP2 and ATARP3 during epidermal development. *Curr Biol.* 2003a;**13**(15):1341–1347. [https://doi.org/10.1016/S0960-9822\(03\)00493-7](https://doi.org/10.1016/S0960-9822(03)00493-7)
- Le J, Mallery EL, Zhang C, Brankle S, Szymanski DB.** *Arabidopsis* BRICK1/HSPC300 is an essential WAVE complex subunit that selectively stabilizes the Arp2/3 activator SCAR2. *Curr Biol.* 2006;**16**(9):895–901. <https://doi.org/10.1016/j.cub.2006.03.061>
- Li C, Mo Y, Wang N, Xing L, Qu Y, Chen Y, Yuang Z, Ali A, Qi J, Fernández V, et al.** The overlooked functions of trichomes: water absorption and metal detoxication. *Plant Cell Environ.* 2023;**46**(3):669–687. <https://doi.org/10.1111/pce.14530>
- Li J, Kim T, Szymanski DB.** Multi-scale regulation of cell branching: modeling morphogenesis. *Dev Biol.* 2019;**451**(1):40–52. <https://doi.org/10.1016/j.ydbio.2018.12.004>
- Li Q, Yin M, Li Y, Fan C, Yang Q, Wu J, Zhang C, Wang H, Zhou Y.** Expression of *Brassica napus* TTG2, a regulator of trichome development, increases plant sensitivity to salt stress by suppressing the expression of auxin biosynthesis genes. *J Exp Bot.* 2015;**66**(19):5821–5836. <https://doi.org/10.1093/jxb/erv287>
- Li Y, Sorefan K, Hemmann G, Bevan MW.** *Arabidopsis* NAP and PIR regulate actin-based cell morphogenesis and multiple developmental processes. *Plant Physiol.* 2004;**136**(3):3616–3627. <https://doi.org/10.1104/pp.104.053173>
- Liang S, Yang X, Deng M, Zhao J, Shao J, Qi Y, Liu X, Yu F, An L.** A new allele of the SPIKE1 locus reveals distinct regulation of trichome and pavement cell development and plant growth. *Front Plant Sci.* 2019;**10**:16. <https://doi.org/10.3389/fpls.2019.00016>
- Lukowitz W, Gillmor CS, Scheible WR.** Positional cloning in *Arabidopsis*. Why it feels good to have a genome initiative working for you. *Plant Physiol.* 2000;**123**(3):795–805. <https://doi.org/10.1104/pp.123.3.795>
- Mathur J, Chua NH.** Microtubule stabilization leads to growth reorientation in *Arabidopsis* trichomes. *Plant Cell.* 2000;**12**(4):465–477. <https://doi.org/10.1105/tpc.12.4.465>
- Mathur J, Mathur N, Kernebeck B, Hülkamp M.** Mutation in actin-related proteins 2 and 3 affect cell shape development in *Arabidopsis*. *Plant Cell.* 2003b;**15**(7):1632–1645. <https://doi.org/10.1105/tpc.011676>
- Mathur J, Mathur N, Kirik V, Kernebeck B, Srinivas BP, Hülkamp M.** *Arabidopsis* CROOKED encodes for the smallest subunit of the ARP2/3 complex and controls cell shape by region specific fine F-actin formation. *Development.* 2003a;**130**(14):3137–3146. <https://doi.org/10.1242/dev.00549>
- Mathur J, Spielhofer P, Kost B, Chua N.** The actin cytoskeleton is required to elaborate and maintain spatial patterning during trichome cell morphogenesis in *Arabidopsis thaliana*. *Development.* 1999;**126**(24):5559–5568. <https://doi.org/10.1242/dev.126.24.5559>
- Morohashi K, Grotewold E.** A system approach reveals regulatory circuitry for *Arabidopsis* trichome initiation by the GL3 and GL1 selectors. *PLoS Genet.* 2009;**5**(2):e1000396. <https://doi.org/10.1371/journal.pgen.1000396>
- Narasimhulu SB, Reddy AS.** Characterization of microtubule binding domains in the *Arabidopsis* kinesin-like calmodulin binding protein. *Plant Cell.* 1998;**10**(6):957–965. <https://doi.org/10.1105/tpc.10.6.957>
- Oppenheimer DG, Pollock MA, Vacik J, Szymanski DB, Ericson B, Feldmann K, Marks MD.** Essential role of a kinesin-like protein in *Arabidopsis* trichome morphogenesis. *Proc Natl Acad Sci USA.* 1997;**94**(12):6261–6266. <https://doi.org/10.1073/pnas.94.12.6261>
- Perroud PF, Quatrano RS.** BRICK1 is required for apical cell growth in filaments of the moss *Physcomitrella patens* but not for gametophore morphology. *Plant Cell.* 2008;**20**(2):411–422. <https://doi.org/10.1105/tpc.107.053256>
- Pesch M, Dartan B, Birkenbihl R, Somssich IE, Hülkamp M.** *Arabidopsis* TTG2 regulates TRY expression through enhancement of activator complex complex-triggered activation. *Plant Cell.* 2014;**26**(10):4067–4083. <https://doi.org/10.1105/tpc.114.129379>
- Reddy AS, Day IS.** The role of the cytoskeleton and a molecular motor in trichome morphogenesis. *Trends Plant Sci.* 2000;**5**(12):503–505. [https://doi.org/10.1016/S1360-1385\(00\)01792-1](https://doi.org/10.1016/S1360-1385(00)01792-1)
- Reddy VS, Reddy AS.** A plant calmodulin-binding motor is part kinesin and part myosin. *Bioinformatics.* 1999;**15**(12):1055–1057. <https://doi.org/10.1093/bioinformatics/15.12.1055>
- Reddy AS, Safadi F, Narasimhulu SB, Golovkin M, Hu X.** A novel plant calmodulin-binding protein with a kinesin heavy chain motor domain. *J Biol Chem.* 1996;**271**(12):7052–7060. <https://doi.org/10.1074/jbc.271.12.7052>
- Saedler R, Mathur N, Srinivas BP, Kernebeck B, Hülkamp M, Mathur J.** Actin control over microtubules suggested by DISTORTED2 encoding the *Arabidopsis* ARPC2 subunit homolog. *Plant Cell Physiol.* 2004a;**45**(7):813–822. <https://doi.org/10.1093/pccp/pch103>
- Saedler R, Zimmermann I, Mutondo M, Hülkamp M.** The *Arabidopsis* KLUNKER gene controls cell shape changes and encodes the AtSRA1 homolog. *Plant Mol Biol.* 2004b;**56**(5):775–782. <https://doi.org/10.1007/s11103-004-4951-z>
- Sambade A, Findlay K, Schäffner AR, Lloyd CW, Buschmann H.** Actin-dependent and -independent functions of cortical microtubules in the differentiation of *Arabidopsis* leaf trichomes. *Plant Cell.* 2014;**26**(4):1629–1644. <https://doi.org/10.1105/tpc.113.118273>
- Schellmann S, Schnittger A, Kirik V, Wada T, Okada K, Beermann A, Thumfahrt J, Jürgens G, Hülkamp M.** TRIPTYCHON and CAPRICE mediate lateral inhibition during trichome and root hair patterning in *Arabidopsis*. *EMBO J.* 2002;**21**(19):5036–5046. <https://doi.org/10.1093/emboj/cdf524>
- Schnittger A, Hülkamp M.** Trichome morphogenesis: a cell-cycle perspective. *Philos Trans R Soc Lond B Biol Sci.* 2002;**357**(1422):823–826. <https://doi.org/10.1098/rstb.2002.1087>
- Schwab B, Mathur J, Saedler R, Schwarz H, Frey B, Scheidegger C, Hülkamp M.** Regulation of cell expansion by the DISTORTED genes in *Arabidopsis thaliana*: actin controls the spatial organization of microtubules. *Mol Genet Genomics.* 2003;**269**(3):350–360. <https://doi.org/10.1007/s00438-003-0843-1>
- Sheahan MB, Rose RJ, McCurdy DW.** Organelle inheritance in plant cell division: the actin cytoskeleton is required for unbiased inheritance of chloroplasts, mitochondria and endoplasmic reticulum in

- dividing protoplasts. *Plant J.* 2004;**37**(3):379–390. <https://doi.org/10.1046/j.1365-313X.2003.01967.x>
- Smith LG, Oppenheimer DG.** Spatial control of cell expansion by the plant cytoskeleton. *Annu Rev Cell Dev Biol.* 2005;**21**(1):271–295. <https://doi.org/10.1146/annurev.cellbio.21.122303.114901>
- Stovold CF, Millard TF, Machesky LM.** Inclusion of Scar/WAVE3 in a similar complex to Scar/WAVE1 and 2. *BMC Cell Biol.* 2005;**6**(1):11. <https://doi.org/10.1186/1471-2121-6-11>
- Szymanski DB.** Arabidopsis trichome morphogenesis: a genetic approach to studying cytoskeletal function. *J Plant Growth Regul.* 2001;**20**(2):131–140. <https://doi.org/10.1007/s003440010014>
- Szymanski DB.** Breaking the WAVE complex: the point of *Arabidopsis* trichomes. *Curr Opin Plant Biol.* 2005;**8**(1):103–112. <https://doi.org/10.1016/j.pbi.2004.11.004>
- Szymanski DB, Marks MD.** *GLABROUS1* overexpression and *TRIPTYCHON* alter the cell cycle and trichome cell fate in *Arabidopsis*. *Plant Cell.* 1998;**10**(12):2047–2062. <https://doi.org/10.1105/tpc.10.12.2047>
- Szymanski DB, Marks MD, Wick SM.** Organized F-actin is essential for normal trichome morphogenesis in *Arabidopsis*. *Plant Cell.* 1999;**11**(12):2331–2347. <https://doi.org/10.1105/tpc.11.12.2331>
- Tian J, Han L, Feng Z, Wang G, Liu W, Ma Y, Yu Y, Kong Z.** Orchestration of microtubules and the actin cytoskeleton in trichome cell shape determination by a plant-unique kinesin. *eLife.* 2015;**4**:e09351. <https://doi.org/10.7554/eLife.09351>
- Tominaga-Wada R, Ishida T, Wada T.** New insights into the mechanism of development of *Arabidopsis* root hairs and trichomes. *Int Rev Cell Mol Biol.* 2011;**286**:67–106. <https://doi.org/10.1016/B978-0-12-385859-7.00002-1>
- Uhrig JF, Mutondo M, Zimmermann I, Deeks MJ, Machesky LM, Thomas P, Uhrig S, Rambke C, Hussey PJ, Hülskamp M.** The role of *Arabidopsis* SCAR genes in ARP2-ARP3-dependent cell morphogenesis. *Development.* 2007;**134**(5):967–977. <https://doi.org/10.1242/dev.02792>
- Wang H, Tong X, Tang L, Wang Y, Zhao J, Li Z, Liu X, Shu Y, Yin M, Adegoke TV, et al.** RLB (RICE LATERAL BRANCH) recruits PRC2-mediated H3K27 tri-methylation on OsCKX4 to regulate lateral branching. *Plant Physiol.* 2022;**188**(1):460–476. <https://doi.org/10.1093/plphys/kiab494>
- Wang S, Barron C, Schiefelbein J, Chen JG.** Distinct relationships between *GLABRA2* and single repeat R2 MYB transcription factors in the regulation of trichome and root hair patterning in *Arabidopsis*. *New Phytol.* 2010;**185**(2):387–400. <https://doi.org/10.1111/j.1469-8137.2009.03067.x>
- Xi XG, Deprez E.** Monitoring helicase-catalyzed DNA unwinding by fluorescence anisotropy and fluorescence cross-correlation spectroscopy. *Methods.* 2010;**51**(3):289–294. <https://doi.org/10.1016/j.ymeth.2010.02.022>
- Yanagisawa M, Alonso JM, Szymanski DB.** Microtubule-dependent confinement of a cell signaling and actin polymerization control module regulates polarized cell growth. *Curr Biol.* 2018;**28**(15):2459–2466. <https://doi.org/10.1016/j.cub.2018.05.076>
- Yanagisawa M, Desyatova AS, Belteton SA, Mallery EL, Turner JA, Szymanski DB.** Patterning mechanisms of cytoskeletal and cell wall systems during leaf trichome morphogenesis. *Nat Plants.* 2015;**1**(3):15014. <https://doi.org/10.1038/nplants.2015.14>
- Yoo SD, Cho YH, Sheen J.** *Arabidopsis* mesophyll protoplasts: a versatile cell system for transient gene expression analysis. *Nat Protoc.* 2007;**2**(7):1565–1572. <https://doi.org/10.1038/nprot.2007.199>
- Zhang X, Dyachok J, Krishnakumar S, Smith LG, Oppenheimer DG.** *IRREGULAR TRICHOME BRANCH1* in *Arabidopsis* encodes a plant homolog of the actin-related protein 2/3 complex activator Scar/WAVE that regulates actin and microtubule organization. *Plant Cell.* 2005a;**17**(8):2314–2326. <https://doi.org/10.1105/tpc.104.028670>
- Zhang X, Grey PH, Krishnakumar S, Oppenheimer DG.** The *IRREGULAR TRICHOME BRANCH1* loci regulate trichome elongation in *Arabidopsis*. *Plant Cell Physiol.* 2005b;**46**(9):1549–1560. <https://doi.org/10.1093/pcp/pci168>
- Zhang C, Mallery EL, Schlueter J, Huang S, Fan Y, Brankle S, Staiger CJ, Szymanski DB.** *Arabidopsis* SCARs function interchangeably to meet actin-related protein 2/3 activation thresholds during morphogenesis. *Plant Cell.* 2008;**20**(4):995–1011. <https://doi.org/10.1105/tpc.107.055350>
- Zhao M, Morohashi K, Hatlestad G, Grotewold E, Lloyd A.** The TTG1-bHLH-MYB complex controls trichome cell fate and patterning through direct targeting or regulatory loci. *Development.* 2008;**135**(11):1991–1999. <https://doi.org/10.1242/dev.016873>